

Final Report on the Optimal Sensor Location

Deliverable 2.6

*Deliverable type: Report
Number: D2.6*

*Actual date of delivery: 9th April 2004
Contractual date: 1st June 2004*

*Task: WP2.6
Responsible: CESAME*

*Dr. Hadyan Fibrianto, Prof. Denis Dochain and Dr. Olivier Schoefs
Centre for Systems Engineering and Applied Mechanics (CESAME)
Université Catholique de Louvain (UCL)
Bâtiment Euler, Avenue Georges Lemaître 4
B-1348 Louvain-la-Neuve, BELGIUM
Emails: fbrianto@csam.ucl.ac.be, dochain@csam.ucl.ac.be*

Reviewers:

<i>Dr. Olivier Bernard</i>	<i>INRIA</i>
<i>Prof. dr. ir. Peter Vanrolleghem</i>	<i>BIOMATH</i>

Factual summary

* D2.3 model-based diagnostics on the VFA, TIC, Alkalinity and gas (CH₄) measurements

- Observability analysis and the observer synthesis
- Numerical simulations for validation
- Applicability of the methodology to the TELEMAC's digester

* Software development for the numerical simulations

* Effort total: 1.1 MM.

Abstract

This deliverable presents the contribution of the CESAME to the WP2, smart sensor development and it completes the previous report (D2.3) about the choice of the optimal sensor location. The study has been carried out on the basis of the available on-line sensors within TELEMAC, i.e. VFA, TIC, alkalinity and CH₄ (Fibrianto *et al.*, 2004) measurements.

The first part of the report recalls the involved reactors in the project and their configurations. The second part deals with some results in D2.3 about the application of the observability measures theory in (Waldruff, *et al.*, 1998) on the PDE model of the anaerobic wastewater treatment process that has been developed from the AM2 model (Schoefs, *et al.*, 2003) with some illustration results based on the implementation of a state observer. These investigations lead to recommendations of the appropriate sensor types, numbers and locations.

The final part is dedicated to the applicability of the proposed methodology to the involved reactors in the TELEMAC project.

Keywords: distributed-parameter model, observability measure, sensor location, VFA/TIC/Z/CH₄ measurements.

Contents

A. Introduction	3
B. Digester types in TELEMAC	4
C. Available sensors within TELEMAC	5
D. Study of the optimal sensor location	5
1. Dynamical model	5
2. Observability of an approximate finite-dimensional model	7
2.1. Observability measure based on the observability matrix singular value	8
2.2. Observability measure based on the observability Gramian singular value	8
2.3. Observability measure based on the Popov-Belevitch-Hautus singular value	8
3. Orthogonal collocation approach	9
3.1. Transformation into a lumped system	9
3.2. Tangent linearization around an operating point	11
4. Implementation of the Observability Measures via numerical simulations	14
4.1. Fixed bed reactor	14
4.2. UASB reactor	23
4.3. Preliminary conclusions of the observability analysis	28
5. Luenberger Observer Synthesis	29
5.1. Application to the fixed bed reactor	29
5.2. Application to the UASB reactor	34
E. Applicability to the TELEMAC reactors	38
F. Conclusions	38
G. References	41

A. Introduction

A key objective of the TELEMAT project is to extract significant information from events occurring on the plant. Data from the sensor network, faults, controller outputs, simulations, and expert advices and opinions are not considered as single and isolated events. They are combined and joined together within the supervision system that incorporates IST tools like expert systems, data mining and Internet technology. The TELEMAT project plans to reduce the need of expert intervention during the regular work of the plant to the minimum. Should live expertise be required, web resources will allow tele-monitoring from the control centre, organised as a network of experts located in different places. This remote expertise pool will be able to supervise, monitor and, if necessary, reconfigure the control policy, at a number of plants. Remote monitoring techniques requires trustful and certain data to compensate the absence of the expert's eye away from the monitored plant. Therefore, the validation module should resolve the uncertainty or at least evaluate it and give a diagnosis that helps the expert in the monitoring centre to take the decision. Also the validation module links to other modules within the project such as the fault detection and isolation module, the database and control modules. Thus, it should provide useful information on the expected standards that guarantee their successful functioning.

Sensors play a crucial role, as the main source of information, in the monitoring system. However, a usual problem in practice is the lack of sensors and/or analyzers. This means and implies a loss of on-line information about the degradation process. In order to overcome this difficulty, model-based state estimation methods (e.g. Kalman or Luenberger observers, or other appropriately designed monitoring tools) can be used to estimate variables that are not available from on-line measurements.

In (Bernard *et al.*, 2001), a reduced-order model, based on two microbial populations and two substrates, has been developed and proved to be reliable and robust, in particular during abnormal operating conditions. One potential drawback of the model is that it assumes the process to behave like a continuously stirred tank reactor. In practice, when using fixed or fluidized bed reactors, in some instances (e.g. in presence of large inlet liquid flow rates, or in absence of information/data about the process variables along the reactor (but then possibly at the price of an additional transport delay term in the dynamical model)), the concentrations of the process components in the liquid phase may be assumed uniform within the reactor, but fixed biomass can be distributed and a biomass gradient can take place. This leads, in some cases, to clogging problems

(Harmand *et al.*, 2002). This has largely motivated the development and validation of a PDE-model for this type of anaerobic digesters (Schoefs *et al.*, 2003).

The observability of a distributed parameter system is not only affected by the choice of sensor but also by the sensor location. It is important to know the appropriate positions in order to obtain the best information about the process dynamics along the reactor. Here we discuss the choice of optimal sensor positions with a predefined number of sensors corresponding to VFA (Volatile Fatty Acid), TIC (Total Inorganic Carbon), alkalinity and gas CH₄ (Fibrianto *et al.*, 2004) measurements. Two reactor configurations will be studied; first is related to the fixed bed reactor (e.g. INRA's digester), and the second one corresponds to the UASB (e.g. USC's digester).

B. Digester types in TELEMAC

As presented in the deliverable D1.1, the available reactors by WP1 partners at lab, pilot and industrial scale are as follows.

USC: A lab scale UASB (L/D= 4.75) is available for the project. A CSTR of 2 litres of useful volume is also available for a shorter period of time. While UASB is fully instrumented, not all measurements on-line could be obtained in experiments carried out in CSTR. The hydrodynamic behaviour of the available UASB by USC was studied in order to evaluate the convenience of using it as a CSTR. This was performed considering that the available industrial reactors were at least designed as CSTR's.

ENEA: an UASB reactor of 600 litres 6 metre tall and with an internal diameter of 0.35 m (L/D= 17) is available for the experimental activities at pilot scale. A recycling loop will be installed for reaching an adequate up-flow velocity.

AGRALCO: An industrial-scale digester that mainly behaves like a Continuous Stirred Tank Reactor (CSTR)(complete mixing type) (2000 m³, 14 m of diameter and 16 m of height, L/D= 1.14) is available. The system is agitated by recycling both liquid and sludge from the bottom to the top of the reactor at a flow rate of 160 m³/h. Besides a pre-industrial CSTR digester (40 m³) is available.

SAUZA: A pre-industrial CSTR reactor (20 m³) is available. An industrial CSTR (5000 m³) has been started up in March, 2002.

DOMECQ BR: An industrial CSTR digester (450 m³) is available.

C. Available sensors within TELEMAC

Referred to the deliverables D2.1, D2.2, D2.4, some sensors that have been developed within TELEMAC are inter alia, VFA (Volatile Fatty Acid), TIC (Total Inorganic Carbon) and alkalinity sensors, using titrimetric analyzers (developed by Applitek, BIOMATH and INRA, it is called “AnaSense” sensor), and also gas analyzer, which is able to provide the percentage of CO₂ and CH₄ on-line.

The optimal sensor location study has been performed on the basis of the above available sensors.

D. Study of the optimal sensor location

1. Dynamical model

All the TELEMAC digesters are assumed to behave like continuously stirred tank reactors (CSTR's). In practice, as it has been mentioned in the introduction, it is not always the case. It depends in particular on the hydrodynamic conditions. When using fixed or fluidized bed reactors, fixed biomass for instance can be distributed and a biomass gradient may exist.

In order to emphasize clogging phenomena and to possibly design and implement tools to avoid clogging problems (Harmand *et al.*, 2002), we have developed a partial differential equation (PDE) model (Schoefs *et al.*, 2003) allowing to account for the axial dispersion in the reactor.

Here, we consider a typical anaerobic WWT process operated in a *fixed-bed* reactor, which is basically composed of two phases, acidogenesis and methanization (Bernard, *et al.*, 2001). The dynamics of the concentrations of the acidogenic and methanogenic biomasses X_1 and X_2 (g VSS/l), respectively, are described by the following equations:

$$\frac{\partial X_1}{\partial t} = (\mu_1 - \alpha D)X_1 \quad (1)$$

$$\frac{\partial X_2}{\partial t} = (\mu_2 - \alpha D)X_2 \quad (2)$$

where α and D are the bacteria fraction in the liquid phase and the effluent dilution rate, respectively. Here, the biomass kinetics, μ_1 and μ_2 , follow Monod-Contois and Haldane-Contois (to account for possible volatile fatty acid (VFA) accumulation) models, respectively:

$$\mu_1 = \frac{\mu_{1\max} S_1}{K_{C1} X_1 + S_1} \quad (3)$$

$$\mu_2 = \frac{\mu_{2s} \cdot S_2}{K_{C2} X_2 + S_2 + \frac{S_2^2}{K_{I2}}} \quad (4)$$

with $\mu_{1\max}$ (day^{-1}), μ_{2s} (day^{-1}), K_{C1} (g COD/g VSS), K_{C2} (mmol VFA/g VSS) and K_{I2} (mmol VFA/g VSS) the biokinetic parameters.

Note that in a fixed bed reactor, as the biomass is attached, the hydrodynamics does not affect directly the biomass. The term αDX_i ($i = 1, 2$) is mainly a detachment term due to the shear forces applied to the biomass by the flow of the liquid in the tank. But in fluidized bed reactors, we have to include the hydrodynamics in the biomass evolution, i.e. there would be a convection term $u_s \partial X / \partial z$ in the equation, where u_s is the superficial solid velocity (different from u_i). It may possibly be advantageously replaced by a term like αDX_i ($i = 1, 2$) used in equations (1) and (2).

An **UASB** reactor can be viewed as a combination of a fixed bed reactor and a fluidized bed reactor; the biomass is fixed in the bottom of the digester (i.e. $\alpha \approx 0$ for $z < h_b$) and free elsewhere outside the filter (i.e. $\alpha = 1$ for $z \geq h_b$), with h_b the blanket thickness.

The time evolution of the concentrations of alkalinity Z (mmol/l), organic substrate S_1 (g COD/l), VFA S_2 (mmol/l), and inorganic carbon C (mmol/l) are represented by the following equations, $\forall z \in [0, H]$,

$$\frac{\partial Z}{\partial t} = -u_l \frac{\partial Z}{\partial z} + \varepsilon_l E_z \frac{\partial^2 Z}{\partial z^2} \quad (5)$$

$$\frac{\partial S_1}{\partial t} = -u_l \frac{\partial S_1}{\partial z} + \varepsilon_l E_z \frac{\partial^2 S_1}{\partial z^2} - k_1 \mu_1 X_1 \quad (6)$$

$$\frac{\partial S_2}{\partial t} = -u_l \frac{\partial S_2}{\partial z} + \varepsilon_l E_z \frac{\partial^2 S_2}{\partial z^2} + k_2 \mu_1 X_1 - k_3 \mu_2 X_2 \quad (7)$$

$$\frac{\partial C}{\partial t} = -u_l \frac{\partial C}{\partial z} + \varepsilon_l E_z \frac{\partial^2 C}{\partial z^2} - q_c + k_4 \mu_1 X_1 + k_5 \mu_2 X_2 \quad (8)$$

where q_c is the CO_2 concentration flow rate (mmol/l/day):

$$q_c(z, t) = k_L a (C + S_2 - Z - K_H P_C) \quad (9)$$

For the above expression, we can express the CO_2 molar flow rate (mmol/day) accumulated at height z as follows:

$$\begin{aligned} Q_c(z, t) &= \int_V q_c dV \\ &= k_L a A \int_0^z (C + S_2 - Z - K_H P_C) d\zeta \end{aligned} \quad (10)$$

with the CO₂ partial pressure, P_C , equal to:

$$P_C(z) = \frac{\phi(z) - \sqrt{\phi(z)^2 - 4K_H P_T(z) \left(C(z) + S_2(z) - Z(z) + \frac{Q_c(z - \Delta z)}{k_L a \cdot A \cdot \Delta z} \right)}}{2K_H} \quad (11)$$

$$\phi(z) = C(z) + S_2(z) - Z(z) - K_H P_T(z) + \frac{Q_M(z) + Q_c(z - \Delta z)}{k_L a \cdot A \cdot \Delta z} \quad (12)$$

Indeed, $P_T(z)$ is the total pressure (atm) at the point z :

$$P_T(z) = P_{atm} + \rho g(H - z) \quad (13)$$

and Q_M is the CH₄ molar flow rate (mmol/day), such as:

$$Q_M(z, t) = k_6 A \int_0^z \mu_2 X_2 d\zeta \quad (14)$$

k_i , $i \in [1, 6]$, are the yield coefficients, $k_L a$ and K_H are the liquid-gas transfer coefficient and the Henry's constant, respectively.

Remark. Note that the integrated values of the CO₂ and CH₄ flow rates on the z first meters are defined as a model assumption to define the measured gas flow rate at z . It does not mean that we have to measure the CO₂ and CH₄ flow rates at all the positions between 0 and z .

The following boundary conditions have also to be added, $\forall t \in \mathbb{R}^+$, $\forall \xi^* = [S_1, S_2, C, Z]$,

$$\begin{cases} \xi^*(z=0, t) = \frac{\xi_{in}^*(t) + R \cdot \xi_{out}^*(t)}{R+1} \\ \frac{\partial \xi^*}{\partial z}(z=H, t) = 0 \end{cases} \quad (15)$$

where $R = Q_{rec} (D \cdot V_{eff})^{-1}$ is the recycle rate with Q_{rec} and V_{eff} , the effluent recycle flow rate and the effective tank volume, respectively.

2. Observability of an approximate finite-dimensional model

Sensor location studies typically refer to quantitative tests based observability tests for a discretized model of the PDE equations of the process (Waldraff, *et al.*, 1998). That's why a discretization scheme, e.g. finite difference or orthogonal collocation, has to be applied to have a finite-dimensional approximation. The observability measure of a finite-dimensional system (Waldraff, *et al.*, 1998) is related to the condition number, or

more specifically to the singular values of the system observability matrix, denoted ϑ , which can be defined different ways (presented in the sequel).

Let us consider the following system representation:

$$\begin{cases} \dot{x} = Ax \\ y = Gx \end{cases} \quad (16)$$

where $x \in \mathbb{R}^n$, $A \in \mathbb{R}^{n \times n}$ and $G \in \mathbb{R}^{m \times n}$, n is the number of state variables and m is the number of measurements.

2.1. Observability measure based on the observability matrix singular value

This method is based on the condition number of the following observability matrix:

$$\vartheta = \begin{bmatrix} G & GA & \dots & GA^{n-1} \end{bmatrix}^T \quad (17)$$

i.e., the ratio between its maximal, denoted $\sigma_{\max}(\vartheta)$, and its minimal singular values, $\sigma_{\min}(\vartheta)$. The observability index is measured by the inverse of the condition number, i.e. $\sigma_{\min}(\vartheta)/\sigma_{\max}(\vartheta)$.

2.2. Observability measure based on the observability Gramian singular value

The Gramian observability matrix is given by:

$$\vartheta_G = \int_0^{\infty} e^{A^T t} G^T G e^{A t} dt \quad (18)$$

The system is completely observable, if and only if:

$$\text{Rank}(\vartheta_G) = n \quad (19)$$

As the previous method, the observability measure of the considered system can also be related to the ratio between $\sigma_{\min}(\vartheta_G)$ and $\sigma_{\max}(\vartheta_G)$.

2.3. Observability measure based on the Popov-Belevitch-Hautus singular value

The observability matrix of Popov-Belevitch-Hautus (PBH) can be written as follows:

$$\vartheta_{PHB}(\lambda_i) = \begin{pmatrix} \lambda_i I - A \\ G \end{pmatrix}; \forall \lambda_i, i=1 \dots n \quad (20)$$

where λ_i is the i^{th} eigenvalue of A . The system is observable if and only if:

$$\text{Rank}(\vartheta_{PHB}(\lambda_i)) = n \quad (21)$$

An equivalent form for observability evaluation of eq. (20) is $\min_{\lambda_i} \frac{\sigma_{\min}(\vartheta_{PHB}(\lambda_i))}{\sigma_{\max}(\vartheta_{PHB}(\lambda_i))}$.

The PBH rank test proposes also another observability measure. If E is the smallest perturbation to the matrix A so as to make the pair $(A+E, G)$ unobservable, the minimal distance to the set of all unobservable pairs $(A+E, G)$ is then given by the solution of the following minimization problem:

$$\|E\|_2 = \min_{s \in \mathcal{C}} \sigma_{\min} \begin{pmatrix} sI - A \\ G \end{pmatrix} \quad (22)$$

The minimization problem (22) is generally non-convex, i.e. difficult to solve. However, the algorithm presented in (Boley, 1990) allows to have upper and lower bounds on $\|E\|_2$. Therefore, the lower bound can be considered as an observability measure.

3. *Orthogonal collocation approach*

3.1. **Transformation into a lumped system**

In the rest of this study, we have considered a weighted residuals method, the orthogonal collocation, to approximate the PDE's into ODE's. They are basically several reasons for selecting this reduction approach (see Waldraff et al, 1998) :

- 1) It has the advantage over finite differences to limit the number of ODE necessary to have to provide a good approximation to a few equations (while typically hundreds of ODE's are needed with finite differences).
- 2) It preserves mass and energy balances; moreover the variables in the reduced model have the same dimension and units than in the original PDE model
- 3) It has also the decisive property in the context of the present study to be a pseudo-spectral method, and with that respect, it is able to transfer almost exactly the spectrum of the original PDE model to the reduced ODE model. This property is very important in the present study since the observability properties of the convection-diffusion-reaction model as the one considered here to describe the dynamics of the anaerobic digesters is characterized e.g. by a loss of observability at the zeros of the system eigenfunctions (see Waldraff et al, 1998).

The orthogonal collocation allows to transform the PDE model into ODE's by expressing the state variables $x(z,t)$ as a finite weighted sum of the state variables at a number $n+1$ of locations called the collocation points:

$$x(z, t) = \sum_{j=0}^n \lambda_j(z) x_j(t); \quad x \in \{S_1, S_2, C, Z, X_1, X_2\} \quad (23)$$

where $x_j(t) = x(z_j, t)$ is the value of x at the collocation point z_j , $j \in [0, n]$, with $0 < z_1 < z_2 < \dots < z_n = H$. $\lambda_j(z_i)$ are the orthogonal functions (e.g. the Lagrange polynomials):

$$\lambda_j(z_i) = \begin{cases} 1 & \text{for } i = j \\ 0 & \text{for } i \neq j \end{cases} \quad \text{or} \quad \lambda_j(z_i) = \lambda_{ij} = \prod_{\substack{j=0 \\ j \neq i}}^n \frac{z - z_j}{z_i - z_j} \quad (24)$$

By applying (23), equations (6), (7), (8) and (5) become, $\forall z_i \in [0, H]$,

$$\frac{dS_{1i}}{dt} = \sum_{j=0}^n (-u_l \dot{L}_{ij} + \varepsilon_l E_z \ddot{L}_{ij}) S_{1j} - k_1 \mu_{1i} X_{1i} \quad (25)$$

$$\frac{dS_{2i}}{dt} = \sum_{j=0}^n (-u_l \dot{L}_{ij} + \varepsilon_l E_z \ddot{L}_{ij}) S_{2j} + k_2 \mu_{1i} X_{1i} - k_3 \mu_{2i} X_{2i} \quad (26)$$

$$\frac{dC_i}{dt} = \sum_{j=0}^n (-u_l \dot{L}_{ij} + \varepsilon_l E_z \ddot{L}_{ij}) C_j + k_L a (K_H P_{Ci} + Z_i - C_i - S_{2i}) + k_4 \mu_{1i} X_{1i} + k_5 \mu_{2i} X_{2i} \quad (27)$$

$$\frac{dZ_i}{dt} = \sum_{j=0}^n (-u_l \dot{L}_{ij} + \varepsilon_l E_z \ddot{L}_{ij}) Z_j \quad (28)$$

Similarly, the biomass equations at the collocation points are written as follows:

$$\frac{dX_{1i}}{dt} = \left(\frac{\mu_{1\max} S_{1i}}{K_{C1} X_{1i} + S_{1i}} - \alpha D \right) X_{1i} \quad (29)$$

$$\frac{dX_{2i}}{dt} = \left(\frac{\mu_{2S} \cdot S_{2i}}{K_{C2} X_{2i} + S_{2i} + \frac{S_{2i}^2}{K_{I2}}} - \alpha D \right) X_{2i} \quad (30)$$

Hence, an ODE nonlinear system can be considered here:

$$\frac{d\xi}{dt} = f(\xi) + A\xi + B\xi_0 \quad (31)$$

where $f(\xi)$ represents the nonlinear term of the model, and

$$\xi = [S_{1,1} \dots S_{1,n} \quad S_{2,1} \dots S_{2,n} \quad C_1 \dots C_n \quad Z_1 \dots Z_n \quad X_{1,1} \dots X_{1,n} \quad X_{2,1} \dots X_{2,n}]^T \quad (32)$$

ξ_0 is the input vector, such as:

$$\xi_0 = [S_{1,0} \quad S_{2,0} \quad C_0 \quad Z_0]^T \quad (33)$$

with the following boundary conditions:

$$\xi_0(t) = \frac{R(t)}{1+R(t)} \xi_n(t) + \frac{1}{1+R(t)} \xi_{in}(t) \quad (34)$$

where $\xi_n = [S_{1,n} \ S_{2,n} \ C_n \ Z_n]^T$, $\xi_{in} = [S_{1,in} \ S_{2,in} \ C_{in} \ Z_{in}]^T$.

Thus, the matrices A and B are:

$$A = \begin{bmatrix} -u_t \Lambda_1 + \varepsilon_l E_z \Lambda_2 & & & & 0 & 0 \\ & -u_t \Lambda_1 + \varepsilon_l E_z \Lambda_2 & & & \vdots & \vdots \\ & & -u_t \Lambda_1 + \varepsilon_l E_z \Lambda_2 & & & \\ & & & -u_t \Lambda_1 + \varepsilon_l E_z \Lambda_2 & & \\ 0 & \dots & & & 0 & 0 \\ 0 & \dots & & & 0 & 0 \end{bmatrix} \quad (35)$$

$$B = \begin{bmatrix} -u_t \Lambda_{10} + \varepsilon_l E_z \Lambda_{20} & & & & \\ & -u_t \Lambda_{10} + \varepsilon_l E_z \Lambda_{20} & & & \\ & & -u_t \Lambda_{10} + \varepsilon_l E_z \Lambda_{20} & & \\ & & & -u_t \Lambda_{10} + \varepsilon_l E_z \Lambda_{20} & \\ 0 & \dots & & & 0 \\ 0 & \dots & & & 0 \end{bmatrix} \quad (36)$$

with

$$\begin{cases} \Lambda_1 = [\dot{L}_{ij}]_{i \in [1,n], j \in [1,n]} \\ \Lambda_2 = [\ddot{L}_{ij}]_{i \in [1,n], j \in [1,n]} \end{cases} \text{ and } \begin{cases} \Lambda_{10} = [\dot{L}_{i0}]_{i \in [1,n]} \\ \Lambda_{20} = [\ddot{L}_{i0}]_{i \in [1,n]} \end{cases} ;$$

where \dot{L} and \ddot{L} are the first and second derivatives of L (i.e. Lagrange polynomial) according to z (i.e. axial position), respectively.

3.2. Tangent linearization around an operating point

Let us now consider a tangent linearization around an operating point, defined by the nominal values of the state vectors and the input vectors, $\bar{\xi}$ and \bar{u} , respectively. If $\delta \xi = \xi - \bar{\xi}$ and $\delta u = u - \bar{u}$, a linear system can be derived, as follows:

$$\frac{d(\delta \xi)}{dt} = \bar{A}(\delta \xi) + \bar{B}(\delta u) \quad (37)$$

where \bar{A} is the Jacobian matrix of the system, which also represents the dynamics of the system around the operating point.

Referring to the model (31) with $u = \xi_{in}$, one can write:

$$\frac{d(\delta\xi)}{dt} = \left(A + \frac{\partial f(\xi)}{\partial \xi} \right) \cdot (\delta\xi) + \frac{R}{1+R} B \cdot (\delta\xi_n) + \frac{1}{1+R} B \cdot (\delta u) \quad (38)$$

If the measured variable(s) satisfy this expression:

$$y = h(\delta\xi) = G \cdot (\delta\xi) \quad (39)$$

then, the study of the system observability can be carried out on the observability matrix, denoted ϑ , which is given by:

$$\vartheta = \begin{pmatrix} G \\ G \left(A + \frac{\partial f(\xi)}{\partial \xi} \right) \\ \vdots \\ G \left(A + \frac{\partial f(\xi)}{\partial \xi} \right)^{n-1} \end{pmatrix} \quad (40)$$

As the Lagrange polynomial L is considered here, at a given instant, one can interpolate the solution at all points from the solutions at collocation points according to:

$$\delta\xi(z) = \sum_{j=0}^n L_j(z) \cdot \delta\xi_j \quad (41)$$

Note that

$$\delta\xi(z_0) = \frac{R}{1+R} \delta\xi(z_n) + \frac{1}{1+R} \delta u \quad (42)$$

$$\delta\xi(z_i) = \sum_{j=1}^{n-1} L_j(z_i) \cdot \delta\xi_j + \left[L_n(z_i) + \frac{L_0(z_i)R}{1+R} \right] \delta\xi_n + \frac{L_0(z_i)}{1+R} \delta u \quad (43)$$

If one locates a sensor at point z_i , the matrix G in equation (39) can be written as follows:

$$G = [0 \quad \dots \quad 0 \quad G_m \quad 0 \quad \dots \quad 0] ; G \in \mathbb{R}^{1 \times 6n} \quad (44)$$

with

$$G_m = [L_1(z_i) \quad \dots \quad L_n(z_i)] + \begin{bmatrix} 0 & \dots & 0 & \frac{L_0(z_i)R}{1+R} \end{bmatrix}$$

Note that the non-zero elements of the matrix G , denoted G_m , depend on the kind of measurement (substrate, inorganic carbon, etc.)

The linearized models corresponding to the measurements of alkalinity Z , organic substrate S_1 , VFA S_2 , and inorganic carbon C can be found in the deliverable D2.3.

For the gas measurement, we shall concentrate on the availability of CH_4 measurement (Fibrianto *et al.*, 2004). As we have a modelling assumption of the CH_4

flow rate value at a given point as described in equation (14), therefore we can define a methane measurement at two points in the reactor as follows:

$$y = h_M(\xi) = Q_M(z_c) - Q_M(z_i) = \frac{k_6 A(z_c - z_i) \xi_2(z_c) \xi_6(z_c)}{K_{C2} \xi_6(z_c) + \xi_2(z_c) + \xi_2^2(z_c)/K_{I2}} \quad (45)$$

where z_c is the nearest collocation point above z_i , $0 \leq z_i < z_c \leq H$. In this case, we can write:

$$h_M = \left[0 \quad \dots \quad \left. \frac{\partial h_M}{\partial \xi_{2C}} \right|_{\xi=\bar{\xi}} \quad \dots \quad \left. \frac{\partial h_M}{\partial \xi_{6C}} \right|_{\xi=\bar{\xi}} \quad \dots \right] \delta \xi \quad (46)$$

with

$$\left. \frac{\partial h_M}{\partial \xi_{2C}} \right|_{\xi=\bar{\xi}} = \frac{k_6 \cdot A \cdot (z_c - z_i) \cdot \mu_{2S} \cdot \bar{\xi}_{6C} \left(K_{C2} \bar{\xi}_{6C} - \frac{\bar{\xi}_{2C}^2}{K_{I2}} \right)}{\left(K_{C2} \bar{\xi}_{6C} + \bar{\xi}_{2C} + \frac{\bar{\xi}_{2C}^2}{K_{I2}} \right)^2} \quad (47)$$

$$\left. \frac{\partial h_M}{\partial \xi_{6C}} \right|_{\xi=\bar{\xi}} = \frac{k_6 \cdot A \cdot (z_c - z_i) \cdot \mu_{2S} \cdot \bar{\xi}_{2C}^2 \left(1 + \frac{\bar{\xi}_{2C}}{K_{I2}} \right)}{\left(K_{C2} \bar{\xi}_{6C} + \bar{\xi}_{2C} + \frac{\bar{\xi}_{2C}^2}{K_{I2}} \right)^2} \quad (48)$$

Note that the choice of a collocation point as one of the sensor locations is arbitrary. Nevertheless, it allows to have z_c closed to z_i , what means that the error between the real measurement value ($Q_M(z_c) - Q_M(z_i)$) and the approximated measurement value ($\frac{k_6 A(z_c - z_i) \xi_2(z_c) \xi_6(z_c)}{K_{C2} \xi_6(z_c) + \xi_2(z_c) + \xi_2^2(z_c)/K_{I2}}$) is minimized.

Note for the Outlet gas flow rate only measurement

As the usual gas sensor is located at the reactor out put, let's also consider a gas (CH_4) flow rate measurement at that position. It can be related to the following expression:

$$y_{gas} = Q_M(z_n = H, t) = k_6 \mu_{2S} A \sum_{j=1}^n \frac{\xi_{2j} \xi_{6j} (z_j - z_{j-1})}{K_{C2} \xi_{6j} + \xi_{2j} + \xi_{2j}^2/K_{I2}} = h_{gas}(\xi) \quad (49)$$

By the linearization procedure, we can deduce:

$$y_{gas} = G_g \cdot \delta \xi = \left. \frac{\partial h_{gas}}{\partial \xi} \right|_{\xi=\bar{\xi}} \delta \xi \quad (50)$$

where the matrix G is represented by:

$$G_g = \left[0_{1 \times n} ; \left[\frac{\partial h_{gas}}{\partial \xi_{2j}} \right]_{j=1..n} ; 0_{1 \times n} ; 0_{1 \times n} ; 0_{1 \times n} ; \left[\frac{\partial h_{gas}}{\partial \xi_{6j}} \right]_{j=1..n} \right] \quad (51)$$

with

$$\frac{\partial h_{gas}}{\partial \xi_{2j}} = \frac{k_6 A (z_j - z_{j-1}) \mu_{2s} \bar{\xi}_{6j} \left(K_{C2} \bar{\xi}_{6j} - \frac{\bar{\xi}_{2j}^2}{K_{I2}} \right)}{\left(K_{C2} \bar{\xi}_{6j} + \bar{\xi}_{2j} + \frac{\bar{\xi}_{2j}^2}{K_{I2}} \right)^2} \quad (52)$$

$$\frac{\partial h_{gas}}{\partial \xi_{6j}} = \frac{k_6 A (z_j - z_{j-1}) \cdot \mu_{2s} \cdot \bar{\xi}_{2j}^2 \left(1 + \frac{\bar{\xi}_{2j}}{K_{I2}} \right)}{\left(K_{C2} \bar{\xi}_{6j} + \bar{\xi}_{2j} + \frac{\bar{\xi}_{2j}^2}{K_{I2}} \right)^2} \quad (53)$$

4. Implementation of the Observability Measures via numerical simulations

4.1. Fixed bed reactor

For the first simulations, the parameter values have been chosen according to the configuration of the INRA fixed bed reactor (Schoeffs et al., 2003). We consider a tubular reactor with a Peclet number, $u_l H / \varepsilon_l E_z$, equal to 20, corresponding to a highly dispersed tubular reactor. Consider that the reactor height H is equal to 3.5 m and its diameter is equal to 0.6 m. The effective volume of the medium is 0.948 m^3 (i.e. $\varepsilon_l = 0.96$). The inlet flow rate is maintained constant, equal to 12.87 l/h . The reactor is operating with a recycle flow rate, i.e. 50 l/h . The atmospheric pressure $P_{atm} = 1.04 \text{ atm}$, the pressure coefficient related to the gravity $\rho g = 0.096841 \text{ atm/m}$, and the temperature is maintained constant, i.e. 35°C . The other parameters are as follows:

Parameter	Value
$\mu_{1\max}$ (day^{-1})	1.2
K_{C1} (g COD/g VSS)	50.5
μ_{2s} (day^{-1})	0.74
K_{C2} (mmol S_2 /g VSS)	16.6
K_{I2} (mmol/l)	256
k_{La} (day^{-1})	19.8
K_H (mol/(l.atm))	16
k_1 (g/g)	42.14

Parameter	Value
k_2 (mmol/g)	250
k_3 (mmol/g)	134
k_4 (mmol/g)	50.6
k_5 (mmol/g)	228.4
k_6 (mmol/g)	244.86
α	0.5
E_z	1

Once the model parameters are defined, we have then computed the three observability measures on the orthogonal collocation model by positioning the sensor at a point, denoted z_s , that moves from 0 to H .

Let us then consider 7 collocation points (including the boundaries, i.e. at 0, 0.16, 0.81, 1.75, 2.69, 3.34, 3.5 m), chosen as the zeros of a Jacobi polynomial with the parameters $(\alpha, \beta) = (0, 0)$ (i.e. Legendre polynomial). It can be shown that this choice is sufficient to obtain a good approximation, especially for the system spectrum, see (Waldruff *et al.*, 1998).

4.1.1. Measuring the gas CH₄ flow rate

From the first observability matrix (see section D.2.1) we can deduce the observability measure as the minimal/maximal singular values ratio for a varying sensor position, $0 \leq z_s \leq H$, as shown by the curves on Figure 1. Figure 2 shows the Gramian observability measure.

Note that both methods result in very low observability indices. These values are therefore not very reliable when related to the numerical accuracy. Nevertheless, the minimal downward “peaks” give us the position where there are observability losses.

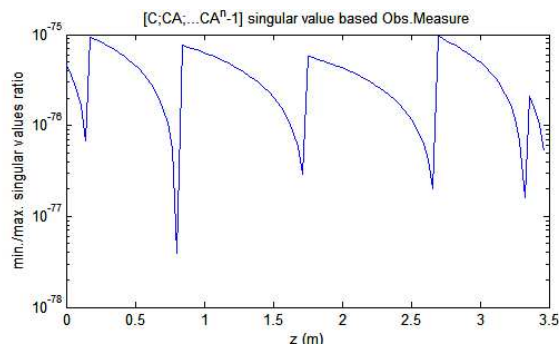


Figure 1. Observability measure based on the usual observability matrix using 7 points.

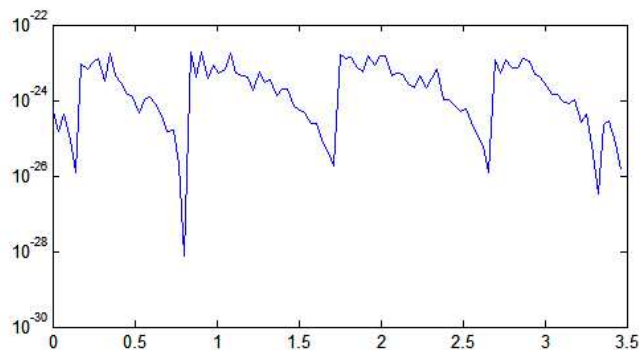


Figure 2. Gramian observability measure using 7 pts.

Let us now consider the PBH method. Figure 3 shows the results from the first and the second PBH methods. As we can see, the observability index values are “better” than the previous ones.

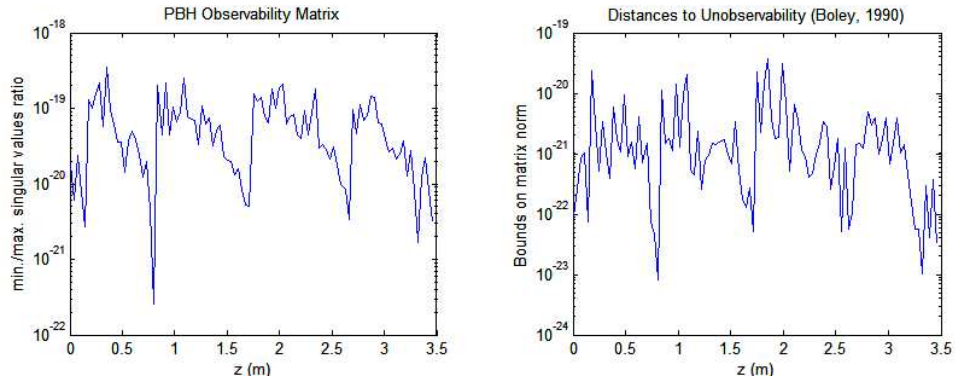


Figure 3. PBH observability measure using 7 points.

Using the three methods, we can note that by considering 7 collocation points there are 5 locations between 0 and H , where there are observability losses. They are 0.1, 0.8, 1.7, 2.7 and 3.3 m.

If we consider 11 collocations points (i.e. 0, 0.06, 0.29, 0.68, 1.18, 1.75, 2.32, 2.82, 3.21, 3.44, 3.5 m), the PBH observability measure gives 9 positions of observability loss, i.e. 0.04, 0.28, 0.67, 1.16, 1.72, 2.31, 2.80, 3.20 and 3.43. Figure 4 illustrates the results of the PBH method. We have also applied the PBH method on a 16 point-model, and this gives 14 locations of observability loss.

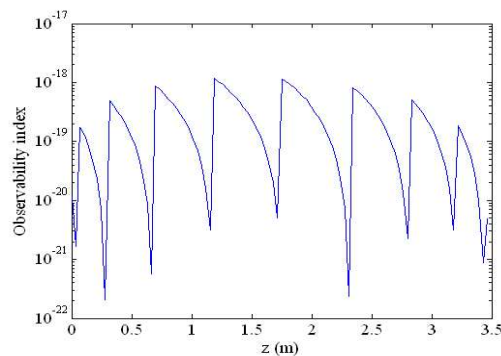


Figure 4. PBH observability measure using 11 points.

These locations approximately correspond to the zeros of the PDE model eigenfunctions (Waldruff, *et al.*, 1998). The larger the model dimension is, the more observability losses may exist. In the sequel, we will only consider the 7-collocation point

model for applying the observability measures. Nevertheless, note that in practice gas measurement is usually done in the gas medium (at the reactor output) because gas measurement in the liquid medium is very difficult to carry out.

4.1.2. Measuring the total inorganic carbon (TIC) concentration

Let us consider the measurement of the total inorganic carbon alone, and then apply the PBH observability measure. Figure 5 shows the results from the first and the second PBH methods, by considering 7 collocation points, identically located as the previous cases.

In this case, the minimal singular values have magnitudes that are higher than the numerical precision of the computing machine, which is of the order of 10^{-14} of magnitude. Observability losses can be noticed at 0.14, 0.43, 0.68 and 0.85 of H , the reactor height (3.5 m).

Indeed, the TIC state variable has a dynamics that depends on all other state variables. Measuring this variable involves knowledge of all other ones.

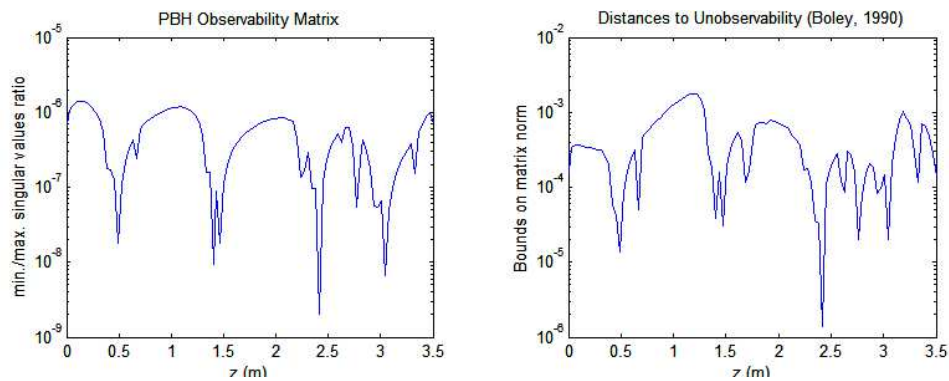


Figure 5. PBH observability measure using 7 collocation points by measuring only the TIC

4.1.3. Measuring the alkalinity

If we measure only the alkalinity, from the first observability matrix (see section D.2.1) we can deduce the observability measure as the minimal/maximal singular values ratio for a varying sensor position, $0 \leq z_s \leq H$, as shown by the curves on Figure 6. We can notice that the observability matrix has a very bad condition number.

By the way, if we apply the other observability measures, i.e. Gramian or PBH (cf. Figure 7), the results will give very low observability indices.

These values are therefore not very reliable when related to the numerical accuracy. Nevertheless we can detect the position where loss of observability may exist, i.e. 0.14, 0.43, 0.68 and 0.85 of H , the reactor height (3.5 m).

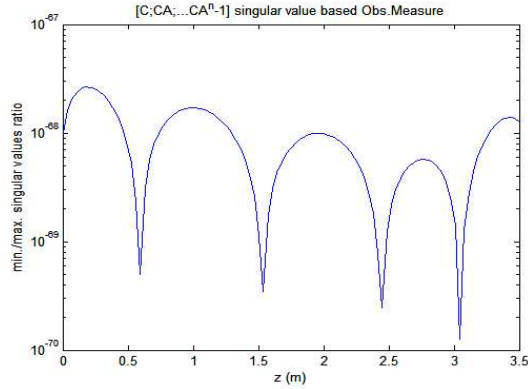


Figure 6. Observability measure on Z (alkalinity) based on the usual observability matrix.

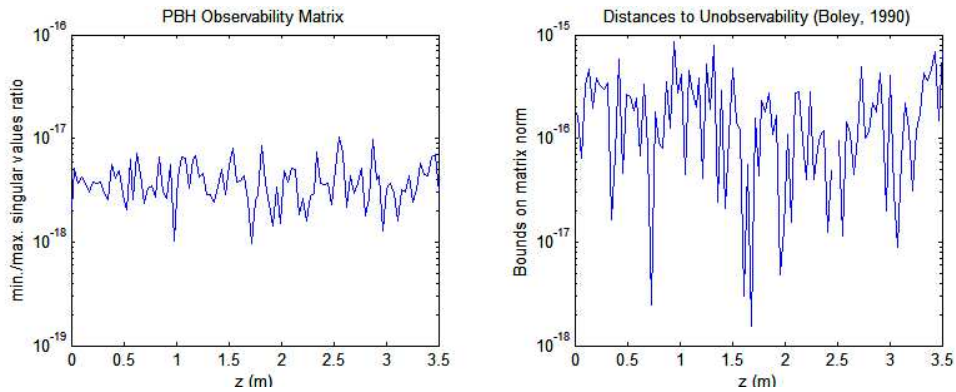


Figure 7. Observability measure on Z (alkalinity) based on the PBH observability matrix.

4.1.4. Measuring the VFA (Volatile Fatty Acid)

If we measure only the VFA, the result will be similar to that of the previous case (alkalinity), cf. Figure 8 and Figure 9. The measurement of the alkalinity or VFA alone does not give the information of all other state variables. This is why the given observability indices are very low.

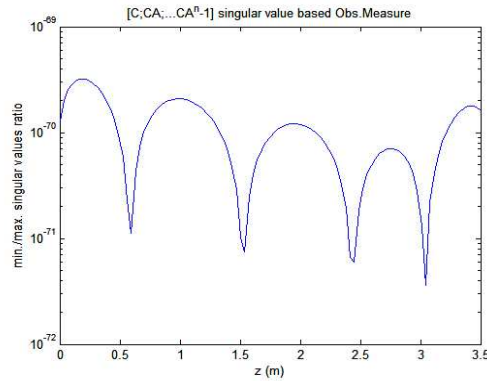


Figure 8. Observability measure on VFA based on the usual observability matrix.

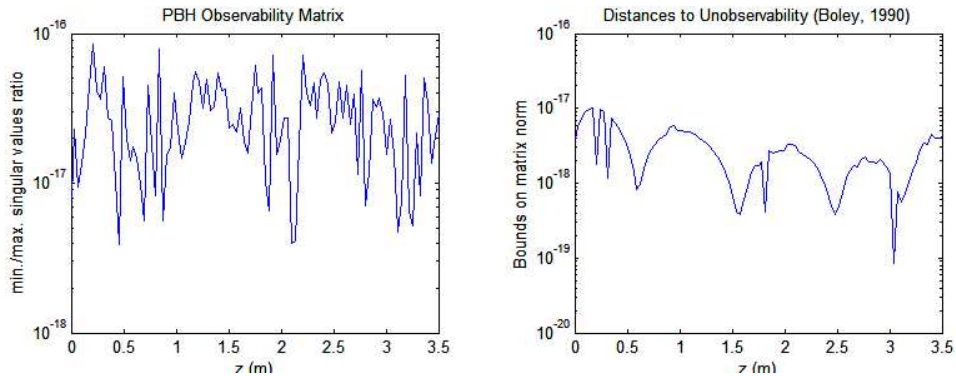


Figure 9. Observability measure on VFA based on the PBH observability matrix.

We have also performed the methodology to the case with more than one type of sensors.

For instance, by combining the COD and VFA measurements, corresponding to the state variables S_1 and S_2 , respectively, the observability measures give similar results (same magnitude) with the case when we only measure the VFA. This result can be explained as follows. The VFA measurement includes also the information of COD. By adding the COD measurement, no new information is added to the observer. Moreover, on-line measurement of COD is not available within the TELEMAC project.

4.1.5. Measuring the TIC and the VFA

Let us consider the combination of the total inorganic carbon and the volatile fatty acid measurements. Figure 10 and Figure 11 show a little enhancement of observability indices (in the term of magnitude) comparing with the obtained result by measuring the TIC alone, but observability losses still can be noticed at the same locations.

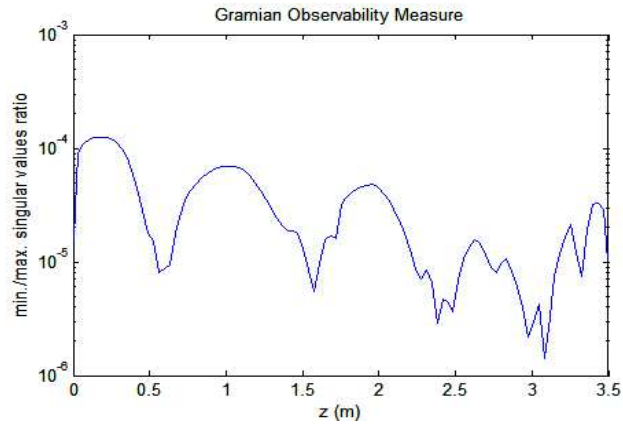


Figure 10. Observability measure on TIC and VFA, based on the Gramian observability matrix.

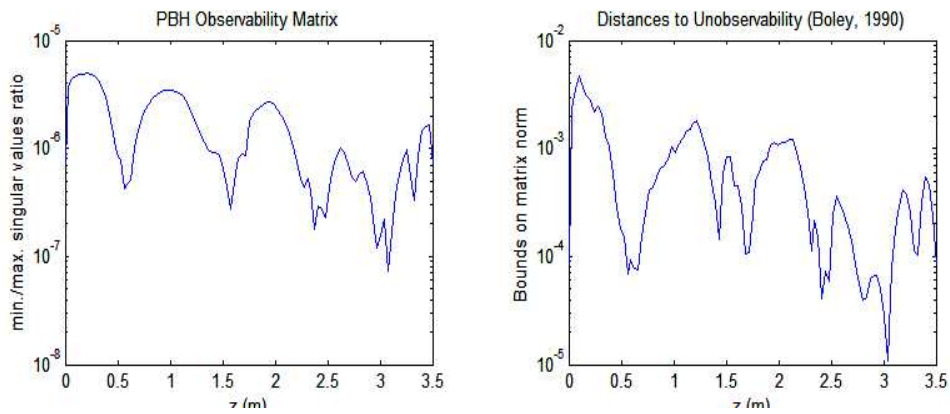


Figure 11. Observability measure on TIC and VFA, based on the PBH observability matrix.

4.1.6. Measuring the TIC and the alkalinity

If we measure the TIC and the alkalinity together, the PBH measure results in the following Figure 12. It can be noticed that the observability indices in this case have a magnitude lightly lower than the previous case (TIC/VFA sensors), especially in the downward peaks, which are located at the same positions.

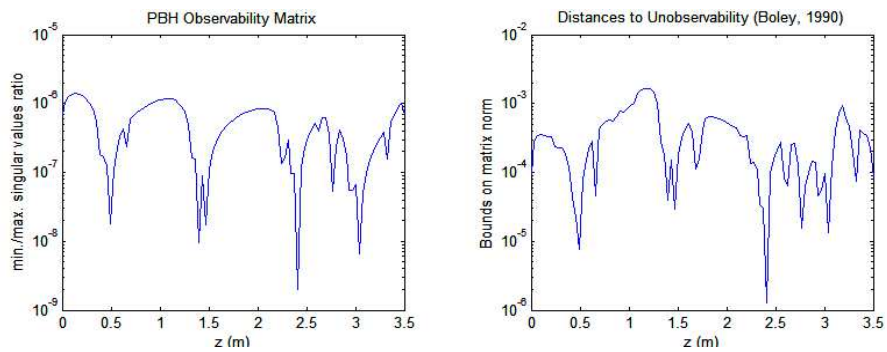


Figure 12. Observability measure on TIC and Z, based on the PBH observability matrix.

4.1.7. Measuring the VFA and the alkalinity

By performing the methodology to the VFA/alkalinity measurements, we find that the observability indices are lower than those of VFA/TIC or TIC/Z measurements. Observability losses can also be noticed at the same places.

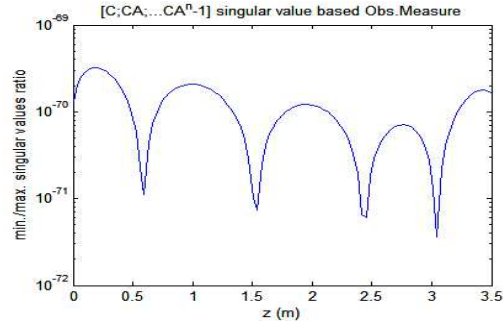


Figure 13. Observability measure on VFA and Z, based on the usual observability matrix.

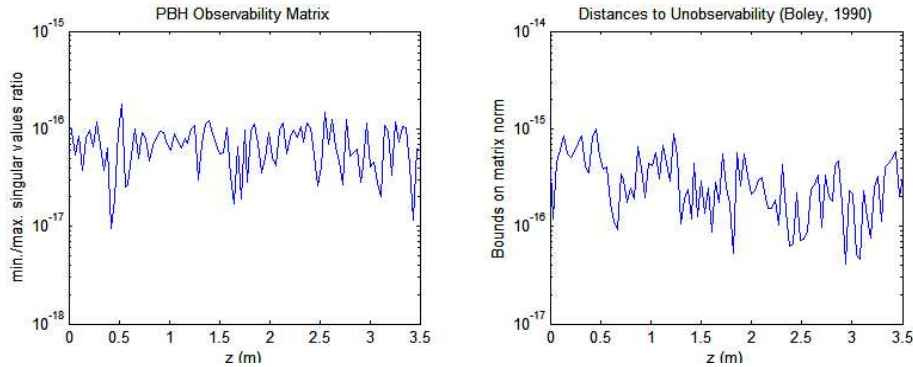


Figure 14. Observability measure on VFA and Z, based on the PBH observability matrix.

4.1.8. Measuring the VFA and the outlet gas

For the measurement combination of VFA concentration and outlet gas flow rate, we can notice in Figure 15 that the observability measures give a lower magnitude than that of VFA/TIC measurements (which is in the order of 10^{-5}).

We can also notice that we cannot distinguish easily the location where losses of observability may exist. Nevertheless we can state that around 1.5 m (or $0.4H$) we have an important loss of observability.

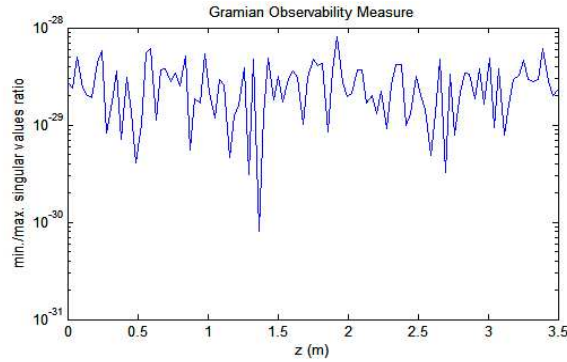


Figure 15. Observability measure on VFA and outlet gas flow rate (q_C), based on the Gramian observability matrix.

4.1.9. Measuring the alkalinity and the outlet gas

Finally, we have applied the observability measures on the alkalinity and the outlet gas flow rate sensors.

In Figure 16 and Figure 17 we can see that the magnitude of the observability indices are almost the same anywhere the alkalinity sensor is located, between 0 and H . In other words, there is almost no loss of observability. Anyway, they are generally lower than the indices resulting from the TIC/VFA, VFA/outlet gas or TIC/Z measurements.

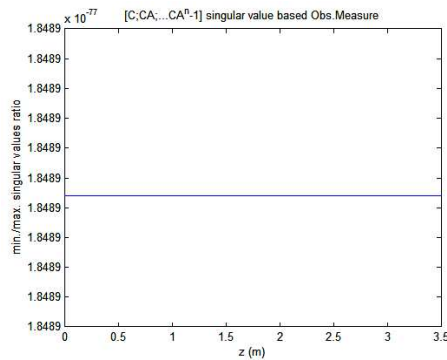


Figure 16. Observability measure on Z and outlet gas flow rate (q_C), based on the usual observability matrix.

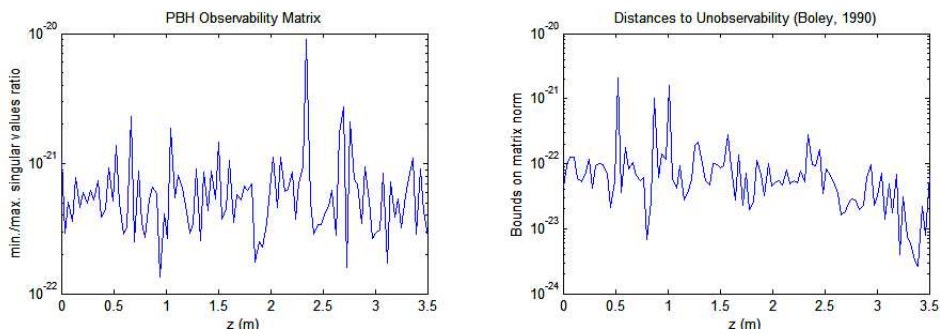


Figure 17. Observability measure on Z and outlet gas flow rate (q_C), based on the PBH observability matrix.

4.1.10. Measuring the TIC, VFA and Alkalinity

Corresponding to the available *AnaSense* in the TELEMAC project, let us consider the combination of the total inorganic carbon, the volatile fatty acid and the alkalinity measurements. Figure 18 and Figure 19 show the same performance as that obtained by measuring the TIC/VFA.

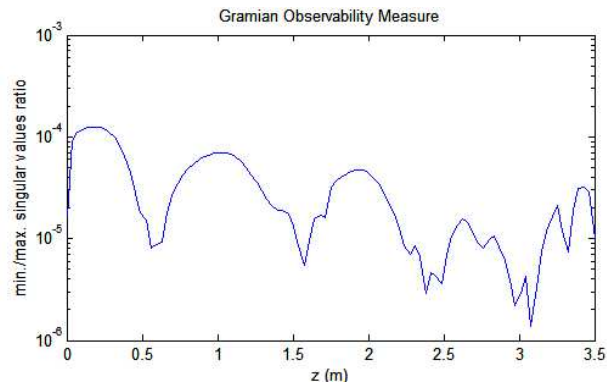


Figure 18. Observability measure on VFA/TIC/Z (AnaSense) based on the Gramian observability matrix.

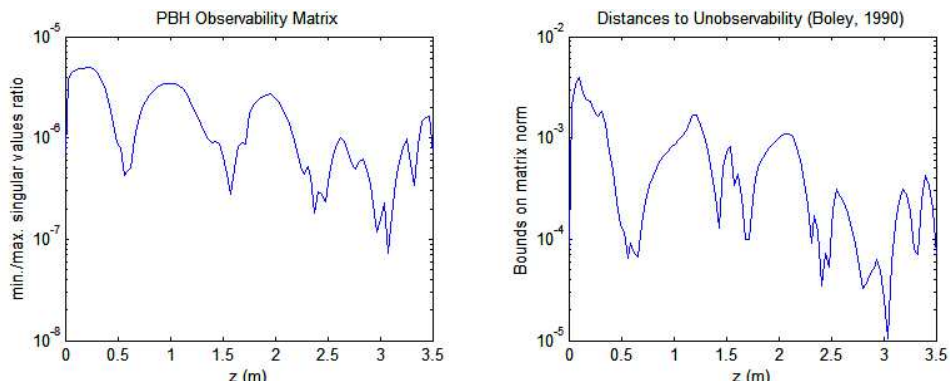
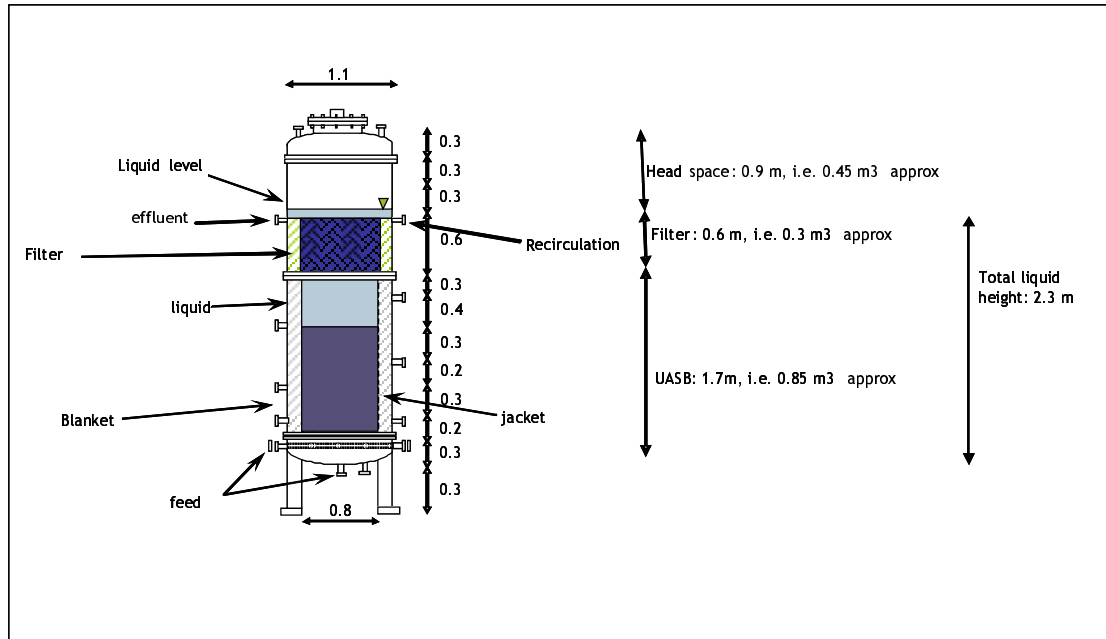


Figure 19. Observability measure on VFA/TIC/Z (AnaSense) based on the PBH observability matrix.

4.2. UASB reactor

The next simulations are dedicated to the configuration of a UASB reactor (e.g. USC's digester). For that, we consider a tubular reactor as shown in Figure 20. The up-flow velocity is around 0.4 – 0.5 m/h.



- All the values are in meters.
- Notice that the head space diameter is 1.1, while the rest of the reactor is 0.8 m.
- To consider the total pressure in the bottom of the reactor consider the liquid height plus the head space pressure, which is normally 100 – 200 mbar

Figure 20. UASB reactor corresponding to USC's digester.

For the other parameters, i.e. kinetics and yield coefficients, we consider the same values as those of the fixed bed reactor. The only changes are related to the value of α in the biomass equations (1) and (2). As it has been previously written in the dynamical model section, an UASB reactor can be considered as a combination of fixed and fluidized bed reactors in cascade; the biomass is fixed in the bottom of the digester and free elsewhere outside the filter, such that the value of α is:

$$\alpha = \begin{cases} 0.1 & \text{for } z \leq h_b \quad (\text{fixed biomass}) \\ 1 & \text{for } h_b < z \leq h_f \quad (\text{free biomass}) \end{cases}$$

with h_b the blanket thickness (1 m). The choice of $\alpha = 0.1$ is arbitrary (yet a value different from zero is necessary in order to allow the existence of steady states different from the wash-out for the biomasses). Note that for $z \geq h_f$, with h_f the position of the filter from the bottom of the reactor (here, 1.7 m), there is no more biomass in the wastewater. Therefore, there is no more dispersion in the liquid medium; a pure time-delay system (associated to a simple plug-flow configuration) can be considered here. With regard to u_l , we can consider a very small time-delay here.

4.2.1. Measuring the total inorganic carbon (TIC)

Like in the fixed-bed case, we have then computed the observability measures on the orthogonal collocation model by positioning the sensor at a point, denoted z_s that moves from 0 to h_f (until the position of the filter). Also we have considered the collocation model with 7 points (here 0, 0.08, 0.39, 0.85, 1.31, 1.62 and 1.70 m).

The results are illustrated in Figure 21 and Figure 22, by using the Gramian and PBH methods, respectively. The observability indices are somewhat lower than those obtained by measuring TIC in a fixed-bed reactor but still relatively high. Fewer downward peaks can be observed here. Remember that the TIC state variable has a dynamics that depends on all other state variable.

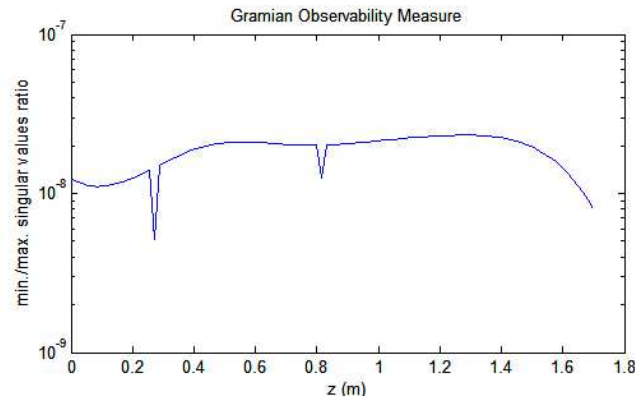


Figure 21. UASB observability index via Gramian method, applied on TIC measurement.

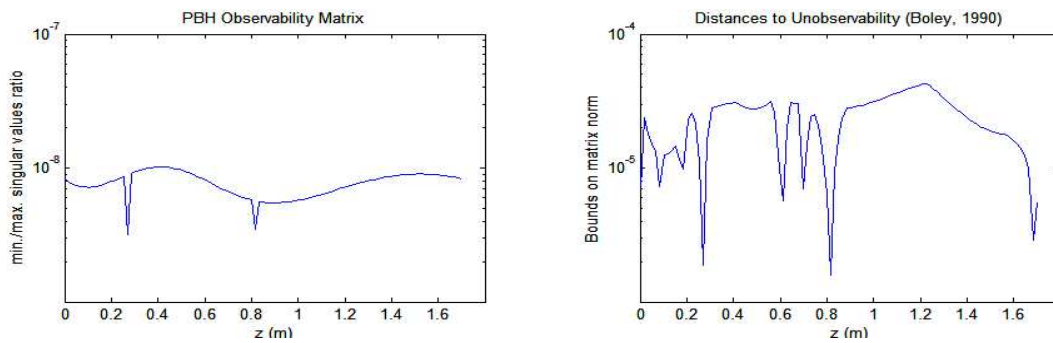


Figure 22. UASB observability index via PBH method, applied on TIC measurement.

4.2.2. Measuring the volatile fatty acid (VFA)

In this case, we can note similar shape of observability indices with those in the fixed-bed reactor, but with significantly lower magnitude (cf. Figure 23 and Figure 24). Losses of observability can be noticed at the same locations, i.e. 0.14, 0.43, 0.68 and 0.85 of H_f .

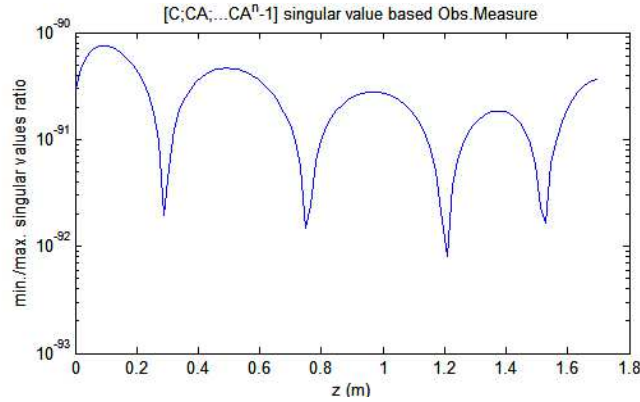


Figure 23. UASB observability index based on the usual observability matrix, applied on VFA measurement.

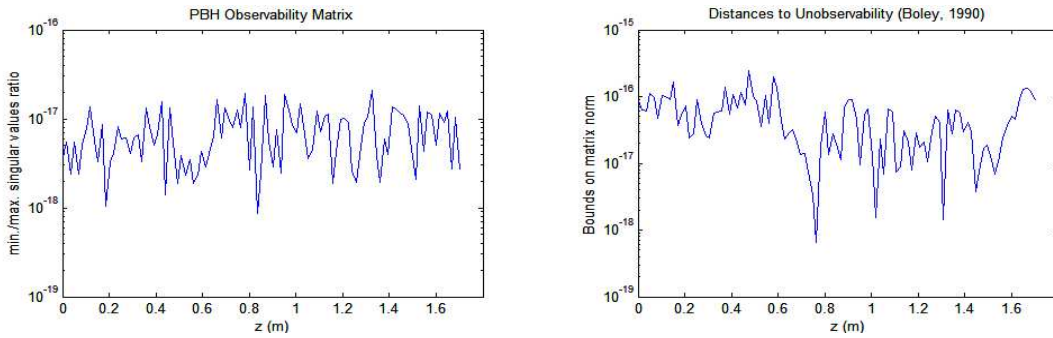


Figure 24. UASB observability index via PBH method, applied on VFA measurement.

4.2.3. Measuring the alkalinity

Applied on the UASB reactor, the alkalinity measurement gives also similar observability indices (see Figure 25 and Figure 26) as those of the fixed-bed reactor but with a lower magnitude. Losses of observability can also be detected at the same positions.

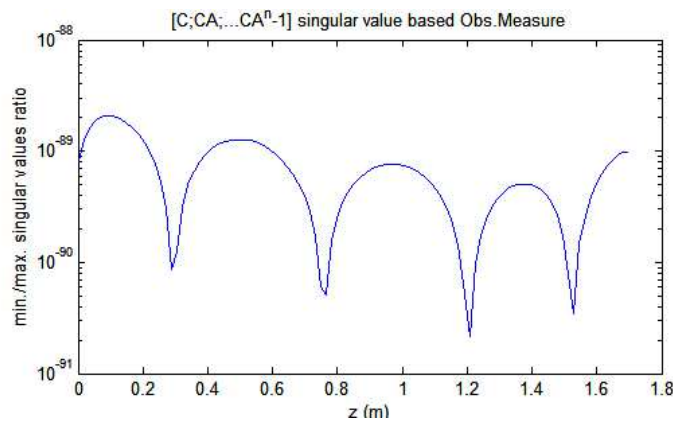


Figure 25. UASB observability index via the usual method, applied on Z measurement.

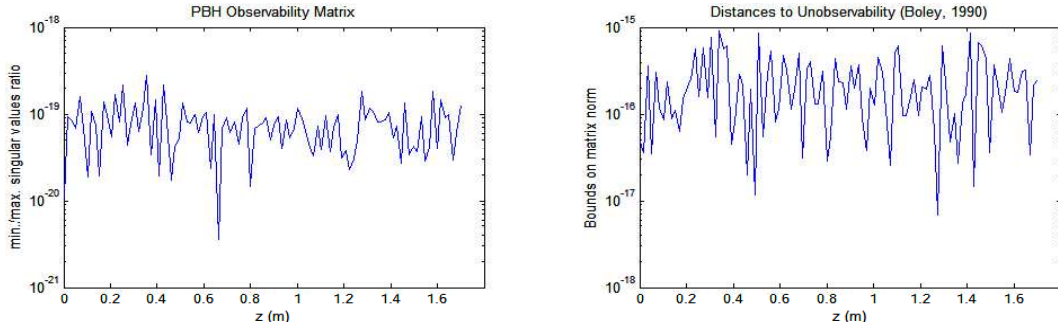


Figure 26. UASB observability index using the PBH method, by measuring the alkalinity.

4.2.4. TIC and VFA measurements

Let us now consider combinations of some measurements. For the combination of TIC and VFA measurements, the observability measures gives the results illustrated in Figure 27 and Figure 28. The magnitudes the observability indices are obviously increased compared to those obtained by measuring TIC or VFA alone. Three locations of observability losses can be noted here, i.e. 0.21, 0.47 and 0.94 of h_f (or in this study case, 0.36, 0.8 and 1.61 m).

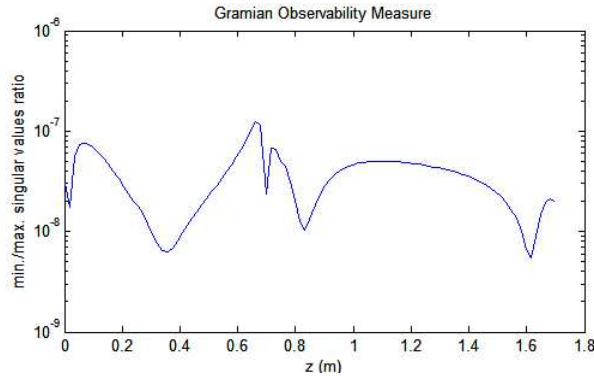


Figure 27. UASB observability index using the Gramian method, by measuring TIC/VFA.

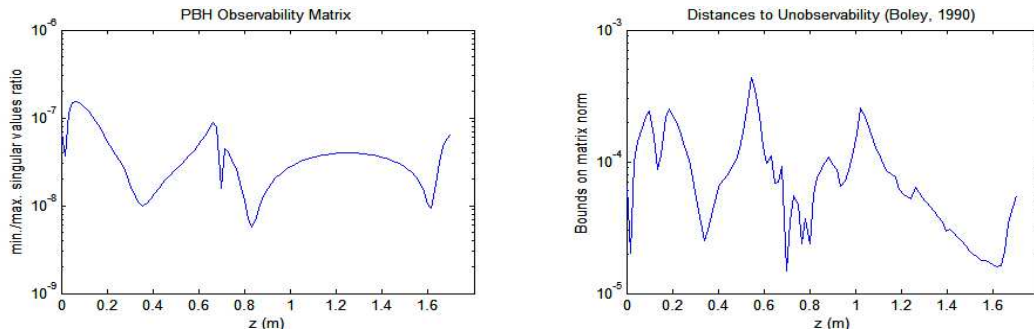


Figure 28. UASB observability index using the PBH method, by measuring TIC/VFA.

4.2.5. TIC, VFA and Z measurements

If we measure TIC, VFA and the alkalinity (these measurements correspond to the developed sensors called AnaSense within the TELEMAC project), the observability tests gives the results illustrated in Figure 29 and Figure 30. The magnitudes the observability indices are exactly the same as those of TIC/VFA measurements.

It can be explained as follows. By adding the alkalinity measurement, no new information is provided. Therefore there is no enhancement of observability values.

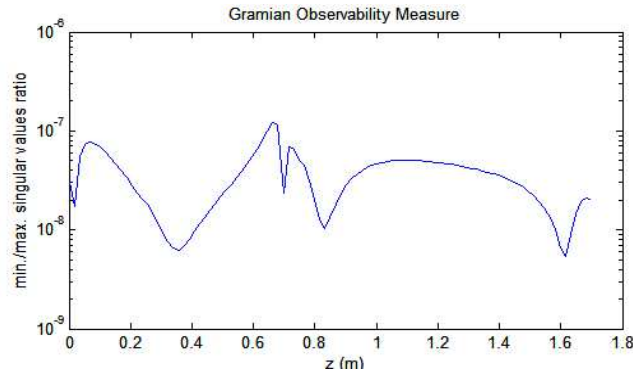


Figure 29. UASB observability index using the Gramian method, by measuring TIC/VFA/Z.

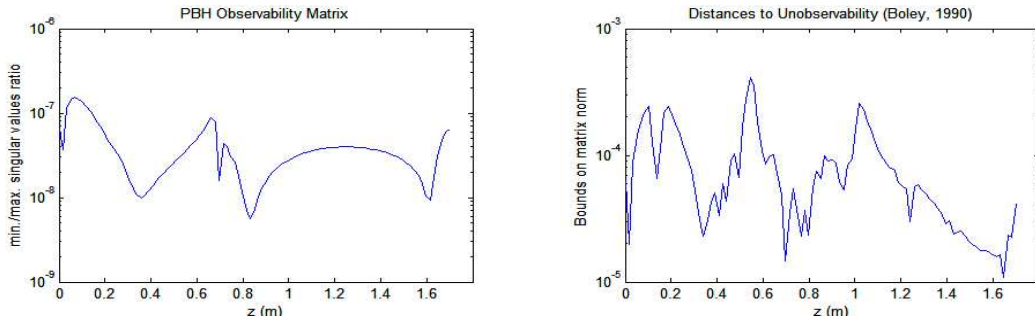


Figure 30. UASB observability index using the PBH method, by measuring TIC/VFA/Z.

4.3. Preliminary conclusions of the observability analysis

The following preliminary conclusions can be drawn from the observability analysis.

- 1) The best zones in terms of observability are somewhere between 10 and 30 cm from the bottom of the reactor. Yet the observability are not significantly decreased for sensors located at the reactor output.
- 2) There is a potential loss of observability at sensor locations corresponding to the zeros of the eigenfunctions of the PDE systems, locations that are given a good accuracy by the pseudo-spectral method used to reduce the PDE model (the orthogonal collocation). In consequence, these locations should be excluded for positioning the sensors.

- 3) There is no such loss of observability at the reactor output for both configurations (fixed-bed and UASB) of the reactor.
- 4) The observability index is not substantially different at the reactor than at the other internal reactor positions. This is mainly the effect of the high liquid flow rate. As a consequence, the locations of the sensors at the reactor output in the reactor configurations (fixed-bed and UASB) of the TELEMAT project are highly recommended, since measurements inside the reactor will not provide substantially improved information.
- 5) The best measurements are clearly TIC and VFA. The observability measures for the other variables are all largely worse.
- 6) The observability index is significantly improved when 2 concentration measurements, the best combinations being TIC/VFA and TIC/alkalinity. By adding a third measurement (alkalinity or VFA, respectively), no improvement of the observability index is obtained.

5. Luenberger Observer Synthesis

For illustrating the observability results at different sensor positions, let us consider a state observer. Here, we propose to use the extended Luenberger observer, which is well adapted to a system evolving around an equilibrium point. The synthesis of the observer is as follows. If the nonlinear model of the process is given by the following state system:

$$\begin{cases} \dot{x}(t) = f(x(t), u(t)) \\ y = g(x(t)) \end{cases} \quad (54)$$

the observer equation will satisfy the equation (55):

$$\frac{d\hat{x}}{dt} = f(\hat{x}(t), u(t)) + K(y(t) - g(\hat{x}(t))) \quad (55)$$

where K is a static gain that is calculated by placing the poles of:

$$\left. \frac{\partial f}{\partial x} \right|_{x_{eq}} - K \left. \frac{\partial g}{\partial x} \right|_{x_{eq}} \quad (56)$$

so as to let the estimation error $(\hat{x}(t) - x(t))$ converges to zero.

5.1. Application to the fixed bed reactor

Assume that the process is initially in steady-state. The initial profiles of the substrates, biomasses and gas flow rates of the WWT process are illustrated on Figure 31. At a given time (here 10 days), steps on the influent concentrations are applied to the process as shown on Figure 32. In this case, the influent pH is maintained constant, at about 5, and so is the influent inorganic carbon, at the value of 0.525 mmol/l.

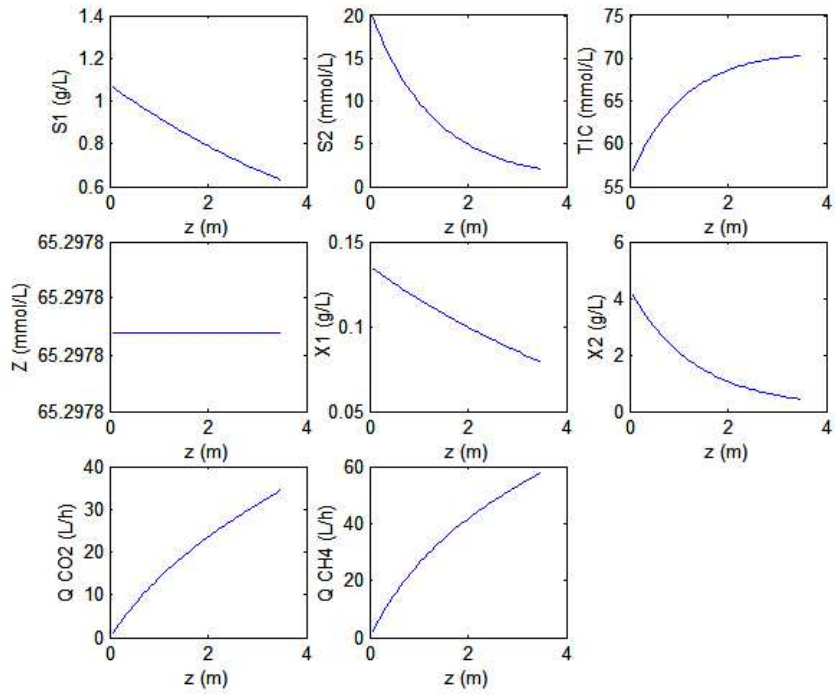


Figure 31. Initial profiles of all the state variables (substrates, products and biomasses) of a WWT process using a fixed-bed reactor.

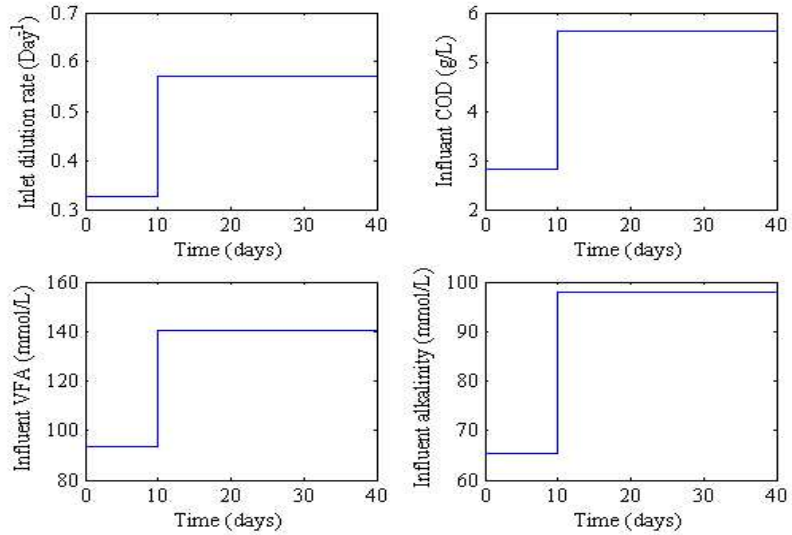


Figure 32. Profiles of the influent parameters of the studied fixed-bed reactor.

5.1.1. Reference model of the fixed-bed reactor

Using these data we have then simulated the model via the finite difference method with 50 nodes, so as to obtain a reference process, which will be considered as the measured variables for the state observer synthesis (cf. Figure 33 and Figure 34). Indeed a finite difference scheme with 50 nodes gives a relatively good accuracy.

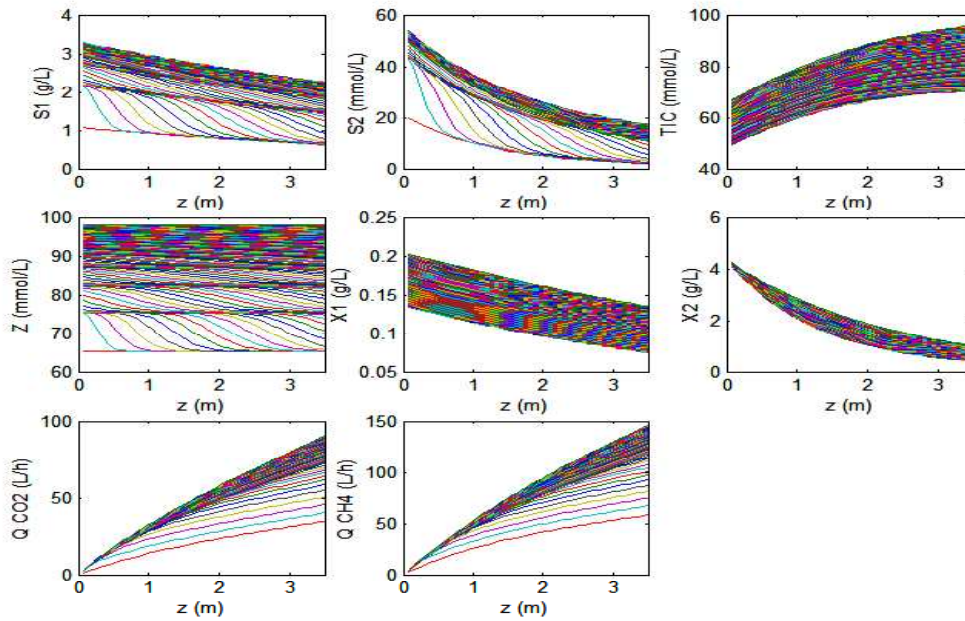


Figure 33. Profiles of the reference states variables a long the fixed-bed reactor.

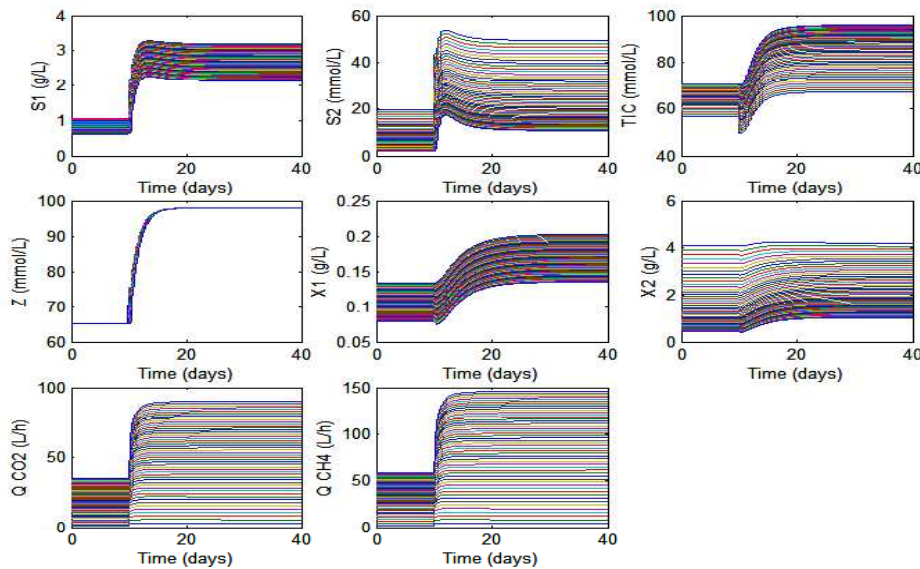


Figure 34. Profiles of the reference state variables in the fixed-bed reactor vs. time.

5.1.2. Observer simulations with CH₄ measurement at 2 positions

First simulations are dedicated to CH₄ measurements when the sensor is located at the positions where observability losses are detected. Here, the Luenberger observer based on the 7-point orthogonal collocation model does not perfectly track the simulated model variable. Figure 35, with a sensor placed on 1.715 m, gives an example of a bad observation. In this case, there is a risk of divergence when there is change of equilibrium, especially if the process is noisy.

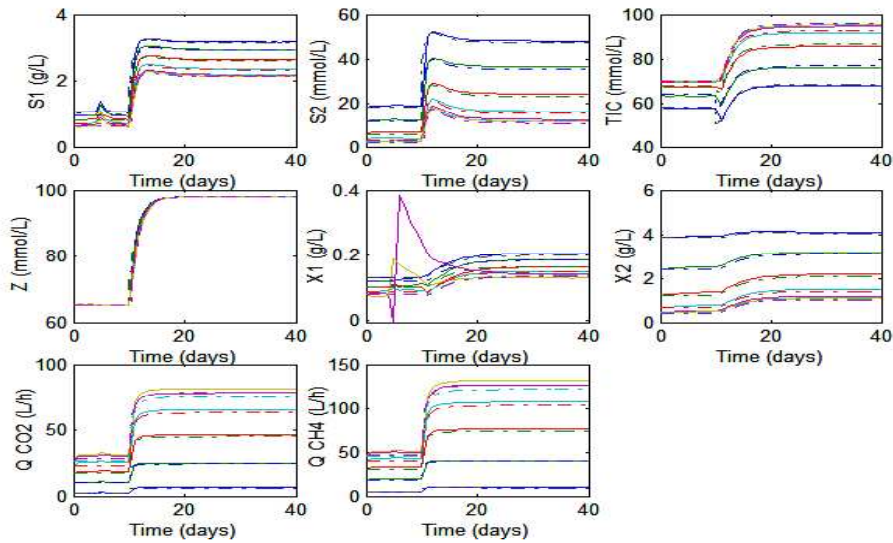


Figure 35. Comparison between the fixed-bed process (dash-dotted lines) and the corresponding observer (continuous lines) by placing the gas CH₄ sensors at 1.715 m and 1.75 m.

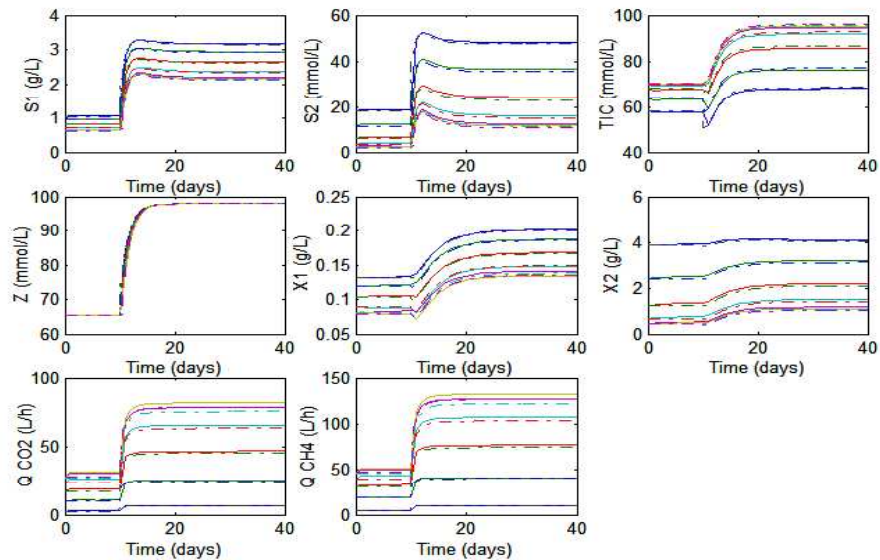


Figure 36. Comparison between the fixed-bed process (dash-dotted lines) and the associated observer (continuous lines) by placing the gas CH₄ sensors at 3.4 m and 3.5 m.

On the other hand, Figure 36 is one example of a good sensor location. We can see in this example that the convergence time after the equilibrium change is good. Small static errors can be noted in the curves between the reference (i.e. finite difference scheme) and estimated (i.e. collocation method) models in the steady-state conditions. Using the finite difference method, the mass conservation law is not totally satisfied because of Taylor approximation. On the other hand, the orthogonal collocation satisfies the mass conservation law.

Note that we have just seen numerical simulations. In practice, a gas measurement in the liquid medium is very difficult to obtain. The only appropriate gas sensor in practice is at the output of the reactor. Nevertheless this investigation allows to warrant that there is no such loss of observability at the reactor output.

Therefore, we have to use the other sensors allowing measurements in liquid medium, such as VFA/TIC/Z sensors. The numerical simulations will also confirm that we need to choose to choose the sensor location in order to avoid some losses of observability.

5.1.3. Observer simulations by measuring TIC/VFA (and Z) at the reactor output

According to our observability analysis, we can state that there is no such loss of observability at the reactor output. Let us now perform simulations using TIC and VFA sensors, located at the reactor output. The results are good (cf. Figure 37). The uses of TIC/alkalinity sensors and TIC/VFA/alkalinity will give similar results.

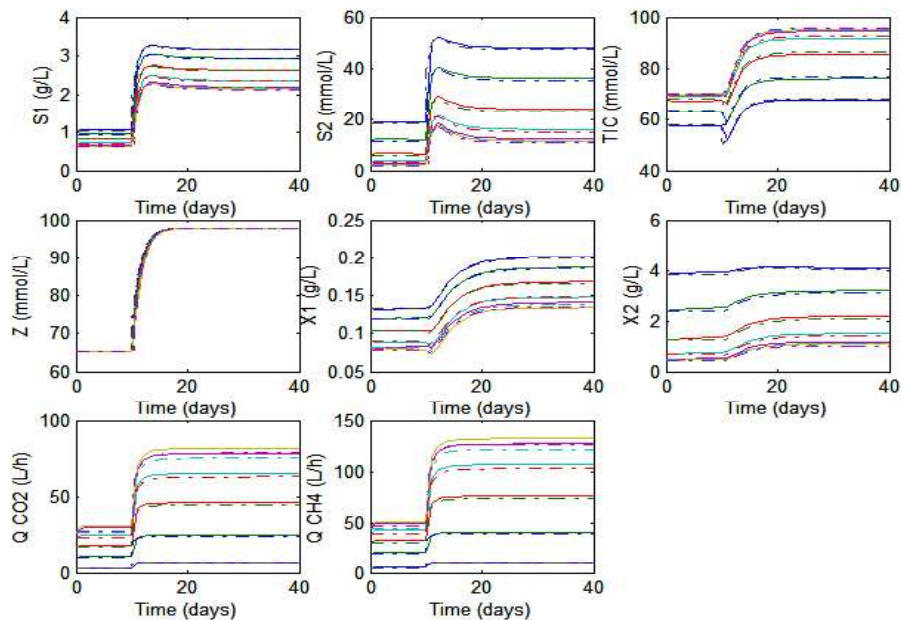


Figure 37. Simulations of the fixed-bed process (dash-dotted lines) and the corresponding observer (continuous lines) by placing the TIC/VFA sensors at H (3.50 m).

5.1.4. Observer simulations with TIC/gas measurements at the reactor output

When we apply the TIC and gas (CH_4) sensors located at the reactor output to the observer, the results are as shown in Figure 38. We can say that the observer works quite good, despite of some numerical errors in the curves.

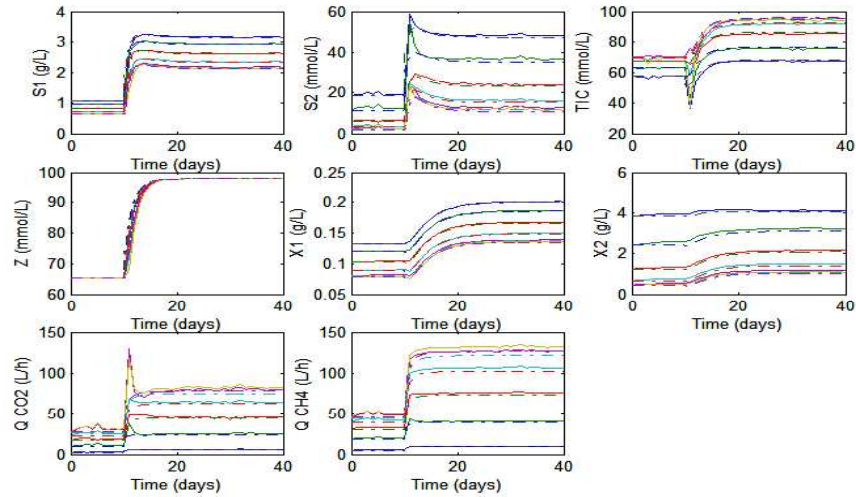


Figure 38. Simulations of the fixed-bed process (dash-dotted lines) and the corresponding observer (continuous lines) by placing the TIC/ CH_4 sensors at H (3.50 m).

5.2. Application to the UASB reactor

Like in the fixed-bed case, we also assume an initial condition in steady-state. The initial profiles of the substrates, biomasses and gas flow rates of the WWT process are illustrated on Figure 39. After 10 days, steps on the influent concentrations represented in Figure 40 are applied to the process. In this case, the influent pH is maintained constant, at about 5, and so is the influent inorganic carbon, at the value of 0.076 mmol/l.

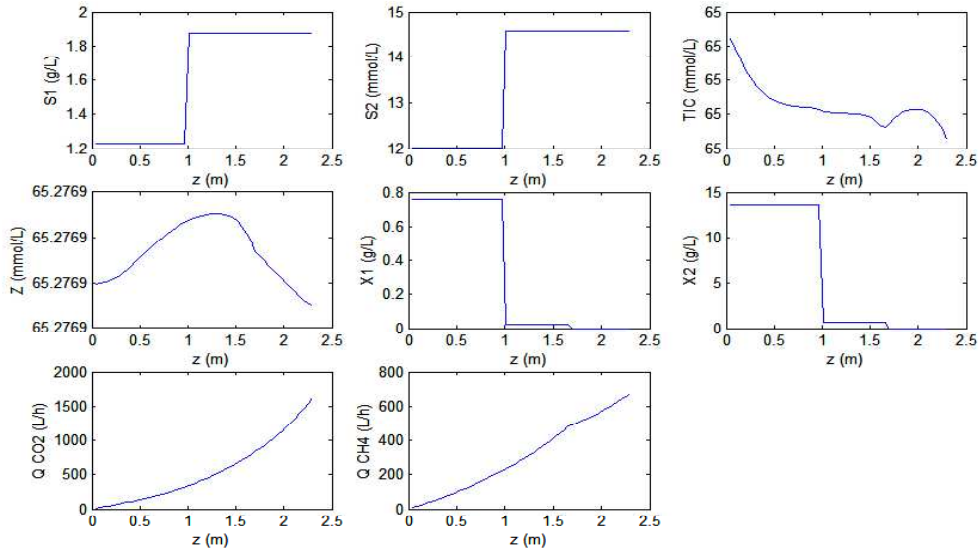


Figure 39. Initial profiles of all the state variables of a WWT process using a UASB reactor.

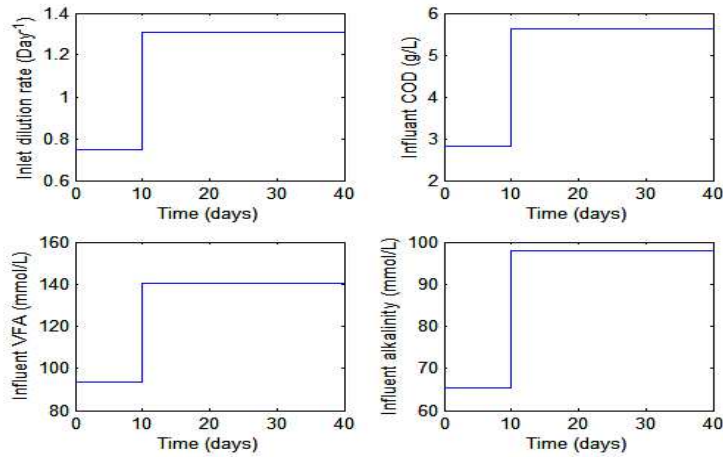


Figure 40. Profiles of the influent parameters of the considered UASB reactor.

5.2.1. Reference model of the UASB reactor

We have then performed the finite difference method with 50 nodes, so as to obtain a reference process. The simulations result in Figure 41 (state variables vs. position in the UASB reactor) and Figure 42 (state variables vs. time). These data will be considered as the measured variables for the state observer synthesis.

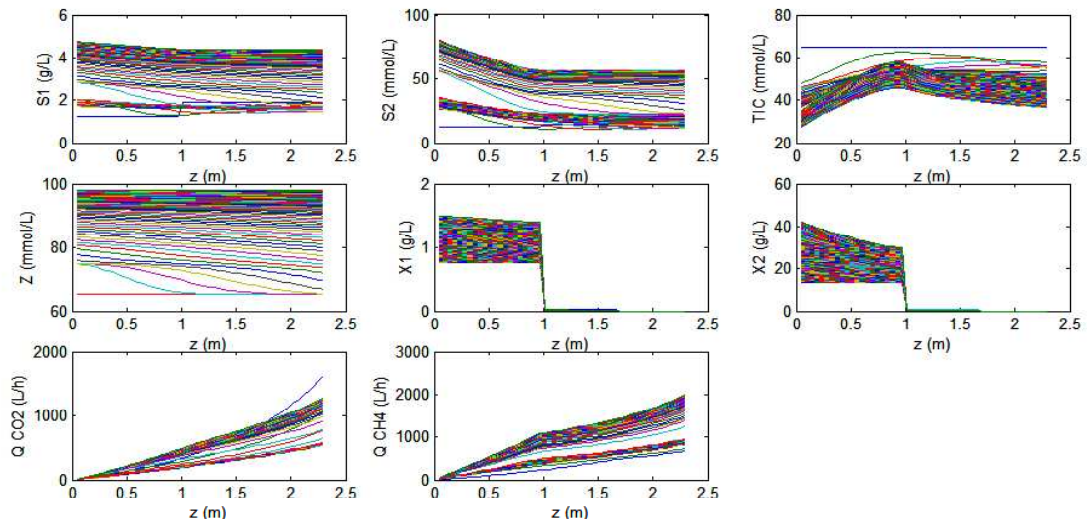


Figure 41. Profiles of the reference states variables a long the UASB reactor.

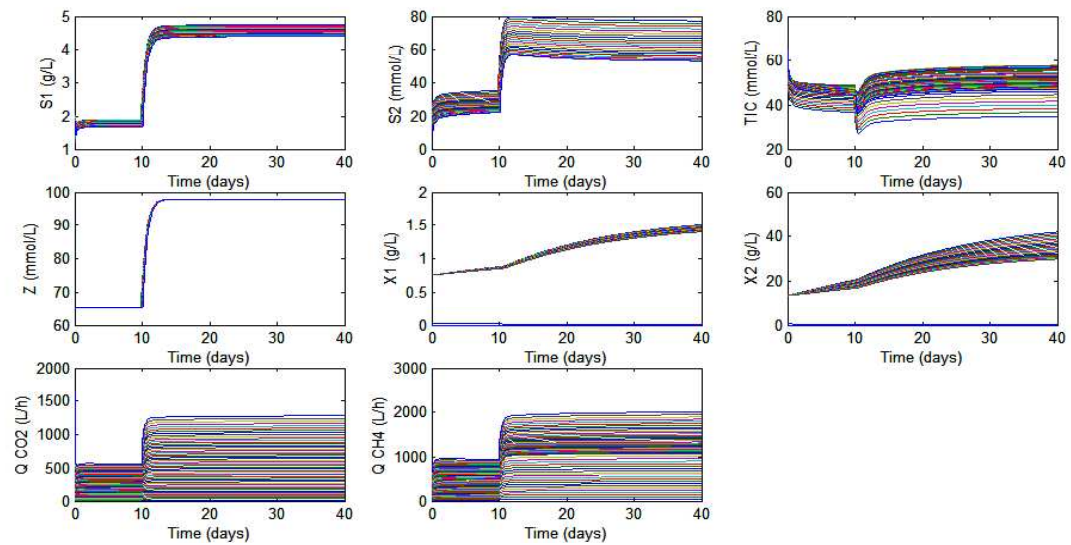


Figure 42. Profiles of the reference state variables in the UASB reactor vs. time.

5.2.2. Observer simulations by measuring TIC

First simulations have been performed using TIC sensor. Let us locate the sensor at h_b (1 m) corresponding to the blanket thickness (the limit between fixed biomass and free biomass). According to the observability analysis, no loss of observability is detected at this location. The simulations have confirmed the validity of our study (cf. Figure 43).

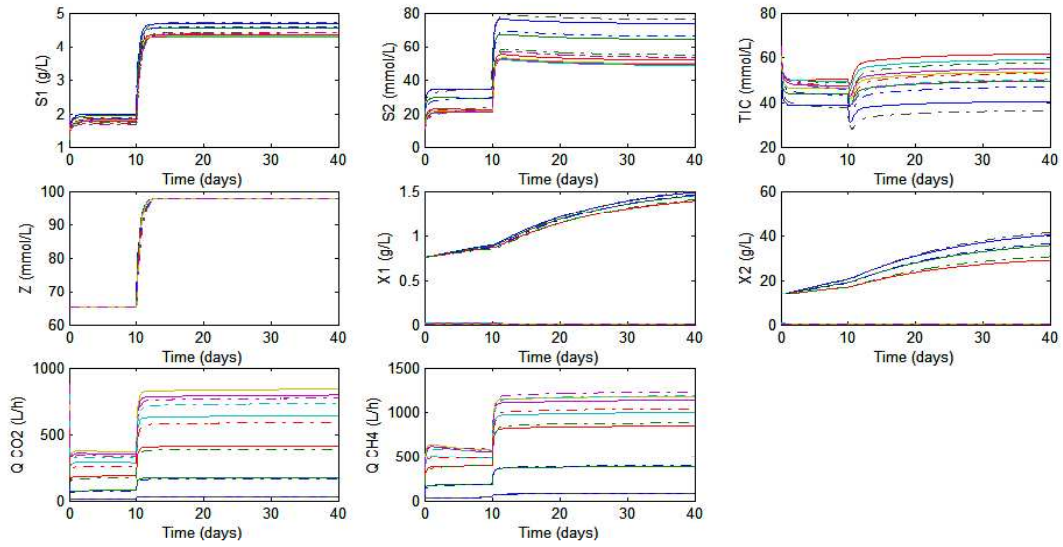


Figure 43. Simulations of the UASB process (dash-dotted lines) and the corresponding observer (continuous lines) by placing the TIC sensor at h_b (1 m).

When the sensor is located at the output of the UASB reactor ($h_f = 1.7$ m), the same performance is obtained (see Figure 44). Indeed, the TIC measurement at $z = H = 2.3$ m (corresponding to the total liquid height in the reactor) will give the same result since there is no dispersion between h_f and H . The only state variable that is not measurable beyond h_f is the biomass.

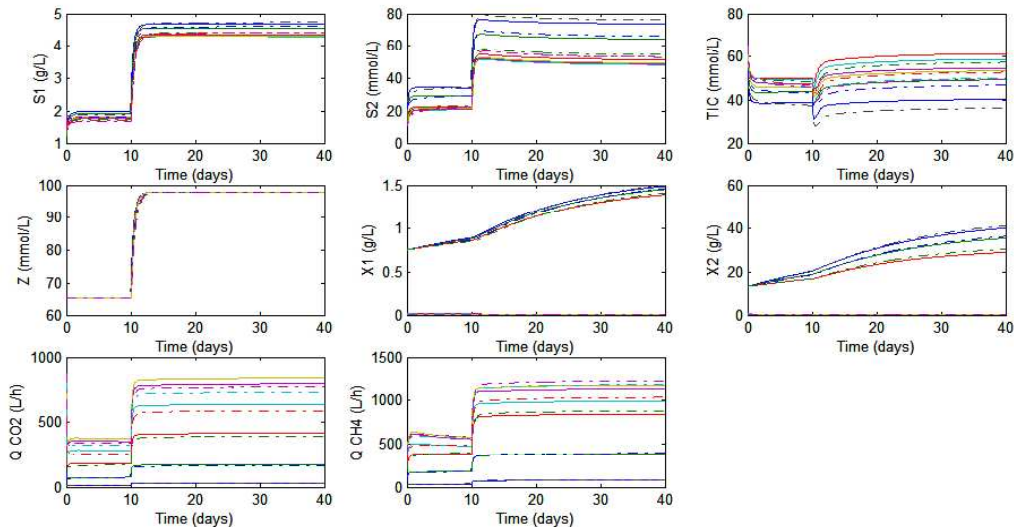


Figure 44. Simulations of the UASB process (dash-dotted lines) and the corresponding observer (continuous lines) by placing the TIC sensor at h_f (1.7 m).

5.2.3. Observer simulations by measuring TIC/VFA/Z at the output of UASB (H_f)

Let us now perform simulations using TIC, VFA and Z sensors (AnaSense). Locate the sensors at h_f (1.7 m) as previously. The simulations have shown (cf. Figure 45). The uses of TIC/alkalinity sensors and TIC/VFA give similar results.

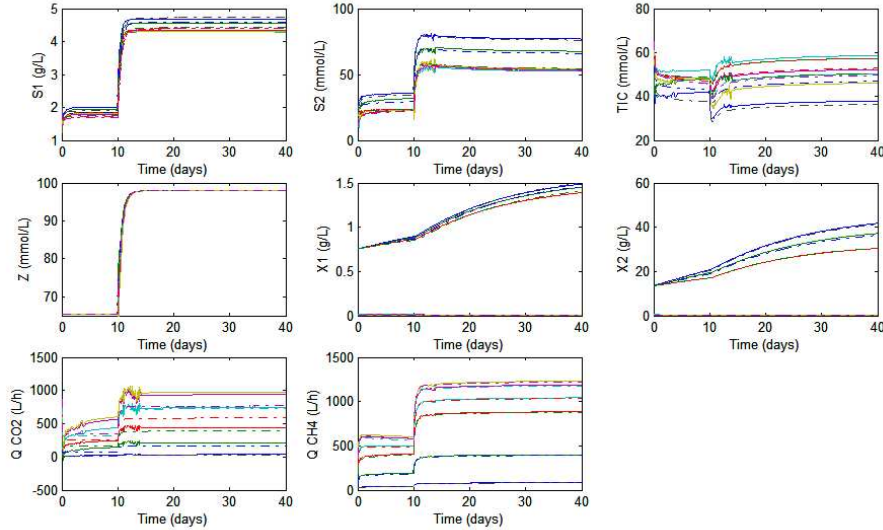


Figure 45. Simulations of the UASB process (dash-dotted lines) and the corresponding observer (continuous lines) by placing the TIC/VFA/Z sensors at h_f (1.7 m).

E. Applicability to the TELEMAT reactors

In these investigations, we have proposed a methodology that allows to choose the sensor location e.g. so as to avoid observability losses while the monitoring is active.

The model has been established according to the general configuration that is used in the TELEMAT digesters. Two of them were considered in this report to illustrate the use of the proposed technique; the first one is related the LBE/INRA digester (fixed-bed configuration) while the second one corresponds to the USC digester (UASB configuration). By changing the numerical values of the reactor configuration, the methodology can also be applied to the other TELEMAT digesters.

F. Conclusions

We have analyzed the sensor location for the TELEMAT digesters using on-line measurable parameters. The analysis is based on system observability tools (Waldraff, *et al.*, 1998) for the PDE model of the processes, corresponding to the LBE/INRA digester (fixed-bed type – Schoefs, *et al.*, 1998) and the USC digester (UASB type). The

methodology that we presented here highlights the locations where observability loss can occur, where the sensors should not be placed.

For a fixed-bed reactor modelled with the following collocation points 0 , $4.69 \times 10^{-2}H$, $0.23H$, $0.5H$, $0.77H$, $0.95H$ and H , with H the height of the reactor, the observability analysis has shown that the system observability is good (or in other words, there is no loss of observability) for the following configuration of sensor(s):

- TIC sensor can be located at a point anywhere except 0.14 , 0.43 , 0.68 and 0.85 of H .
- VFA or Z sensor gives very bad observability indices. Moreover, we note also losses of observability at the same locations as those of TIC measurement.
- CH₄ (methane) gas sensor alone has to be placed at 2 positions. One sensor is placed at a collocation point and the other one must be placed below the considered collocation point, except $2.86 \times 10^{-2}H$, $0.2H$, $0.45H$, $0.7H$ or $0.9H$ corresponding to the points where loss of observability may exist.
- When several sensors are combined, the best combination is TIC/VFA measurements. Nevertheless, there may be losses of observability in some locations mentioned previously.
- It is also possible to have the combination between TIC and alkalinity sensors, or TIC, VFA and alkalinity. The use of the AnaSense sensor that measures TIC, VFA and Z is then recommended. Nevertheless, the following locations: 0.14 , 0.43 , 0.68 and 0.85 of H , have to be avoided.

In the UASB case, the results are quite similar with the previous one. We have modelled using a 7-point-collocation model, applied the three observability measures and noted the following statements:

- When only the TIC is measured, less losses of observability can be noticed. The observability index is quite uniform along the reactor.
- The measurements of VFA alone or alkalinity alone result in very bad observability indices. Therefore they are not recommended.
- When we combine TIC and VFA, the observability index is improved, but we have some observability losses at 0.21 , 0.47 and 0.94 of H_f .
- The addition of the alkalinity measurement in the TIC/VFA measurement does not improve the quality of observability, since no new information is provided by Z measurement.

- The best zones in terms of observability are somewhere between 10 and 30 cm from the bottom of the reactor. Yet the observability are not significantly decreased for sensors located at the reactor output.

The results of this study are illustrated in numerical simulations by implementing a state observer, i.e. the extended Luenberger observer. Note that the state observer is designed by using the orthogonal collocation method, while the reference model is using a finite difference scheme.

When one sensor is located at the positions where observability losses are detected by the mentioned observability measures, there is a risk of divergence in transient conditions, especially if the process is noisy; the state observer cannot follow perfectly the reference model.

On the other hand, when we avoid these positions, the convergence time of the observer response after the equilibrium change is good.

Indeed the collocation method is a pseudo-spectral method. Therefore, it transfers approximately the spectrum of the PDE equation. The observability losses are related to the zeros of the PDE model eigenfunctions. Hence, their number and positions depend on the model dimension. Our investigation has shown that a 7-point-collocation model is the best compromise between accuracy and least of observability losses.

Finally, the following important conclusions can be drawn.

- 1) There is a potential loss of observability at sensor locations corresponding to the zeros of the eigenfunctions of the PDE systems, locations that are given a good accuracy by the pseudo-spectral method used to reduce the PDE model (the orthogonal collocation). In consequence, these locations should be excluded for positioning the sensors.
- 2) There is no such loss of observability at the reactor output for both configurations (fixed-bed and UASB) of the reactor.
- 3) The observability index is not substantially different at the reactor than at the other internal reactor positions. This is mainly the effect of the high liquid flow rate. As a consequence, the locations of the sensors at the reactor output in the configurations (fixed-bed and UASB) of the TELEMAC project are highly recommended, since measurements inside the reactor will not provide substantially improved information.
- 4) The best measurements are clearly the TIC and the VFA. The observability measures for the other variables (alkalinity, CO₂ and CH₄ flow rates) are all largely worse.
- 5) For the UASB, the best zones in terms of observability are somewhere between 10 and 30 cm from the bottom of the reactor. Yet the observability are not significantly decreased for sensors located at the reactor output.

- 6) The observability index is significantly improved when considering at least 2 concentration measurements, the best combinations being TIC/VFA and TIC/alkalinity. The combination of TIC/VFA/alkalinity measurements will give results as good as those obtained by the two previous combinations.
- 7) In conclusion, the AnaSense sensor (measuring TIC/VFA/Z together) is recommended in both fixed-bed and UASB reactors and can be located at the reactor output.

G. References

- Bernard O., Z. Hadj-Sadok, D. Dochain, A. Genovesi, and J.-P. Steyer, 2001. "Dynamical Model Development and Parameter Identification for an Anaerobic Wastewater Treatment Process," *Biotechnol. Bioeng.*, Vol. 75, p. 424-438.
- Boley D., 1990. "Estimating the sensitivity of the algebraic structure of pencils with simple eigenvalue estimates", *SIAM Journal of Matrix Analysis Applications*, Vol. 11, N° 4, p. 632-643.
- Fibrianto H., D. Dochain and O. Schoefs, 2004. "Optimal sensor location based on the observability measure for an aerobic wastewater treatment process", in *the 9th International Symposium on Computer Applications in Biotechnology (CAB9)*, Nancy, France, March 28-31.
- Schoefs O., D. Dochain, H. Fibrianto and J.-P. Steyer, 2003. "Modelling and identification of a distributed-parameter anaerobic wastewater treatment process", in *the Multiconference on Computational Engineering in Systems Applications (CESA 03)*, July 9-11, Lille, France.
- Waldruff W., D. Dochain, S. Bourrel and A. Magnus, 1998. "On the use of observability measures for sensor location in tubular reactor", *Journal of Process Control*, Vol. 8, N° 5-6, p. 497-505.